Ocean Sci. Discuss., 11, 331–390, 2014
www.ocean-sci-discuss.net/11/331/2014/
doi:10.5194/osd-11-331-2014

Ocean Science
Discussions
Open Access

Qualified temperature, salinity and dissolved oxygen climatologies in a changing Adriatic Sea

M. Lipizer[1], **E. Partescano**[1], **A. Rabitti**[1,*], **A. Giorgetti**[1], **and A. Crise**[1]

[1]OGS – Istituto Nazionale di Oceanografia e di Geofisica Sperimentale, Trieste, Italy
[*]now at: NIOZ Royal Netherlands Institute for Sea Research, Texel, the Netherlands

Received: 16 December 2013 – Accepted: 13 January 2014 – Published: 3 February 2014

Correspondence to: M. Lipizer (mlipizer@ogs.trieste.it)

Published by Copernicus Publications on behalf of the European Geosciences Union.

Abstract

An updated climatology, based on a comprehensive dataset (1911–2009) of temperature, salinity and dissolved oxygen, has been produced for the whole Adriatic Sea with the Variational Inverse Method using the DIVA software. Climatological maps were produced at 26 levels and validated with Ordinary Cross Validation and with real vs. synthetic Temperature–Salinity diagram intercomparison. The concept of Climatology–Observation Misfit (COM) has been introduced as an estimate of the physical variability associated with the climatological structures. In order to verify the temporal stability of the climatology, long-term variability has been investigated in the Mid Adriatic and the South Adriatic Pits, regarded as the most suitable records of possible long-term changes. Compared with previous climatologies, this study reveals a surface temperature rise (up to 2 °C), a clear deep dissolved oxygen minimum in the South Adriatic Gyre and a bottom summer oxygen minimum in the North Adriatic. Below 100 m all properties profoundly differ between the Middle and the South Adriatic. The South Adriatic Pit clearly shows the remote effects of the Eastern Mediterranean Transient, while no effect is observed in Middle Adriatic Pits. The deepest part of the South Adriatic seems now to be significantly saltier (+0.18 since the period 1911–1914, with an increase of +0.018 decade^{-1} since the late 1940s) and warmer (+0.54 °C since 1911–1914), even though a long-term temperature trend could not be statistically demonstrated. Conversely, the Middle Adriatic Pits present a long-term increase in apparent oxygen utilisation (+0.77 mL L^{-1} since 1911–1914, with a constant increase of +0.2 $\text{mL L}^{-1}\,\text{decade}^{-1}$ after the 1970s).

1 Introduction

Nowadays many applications in the marine research field, as well as in the maritime management sector, require climatologies, i.e. fields of major ocean parameters averaged over a period of time. Reliable estimates of the environmental baselines, climatic trend estimates, improved initial conditions for numerical models and requirements for environmental status assessment according to European Environmental Policies (e.g. Water Framework Directive WFD-2000/60/EC; Marine Strategy Framework Directive, MSFD-2008/56/EC) are just a few relevant examples of such applications. However, the climatology per se provides only an estimate of "average" fields, without explicitly showing the intrinsic dynamics connected with the short-term and long-term variability that measurements naturally incorporate. A knowledge of the uncertainty associated with the approximation algorithms used in producing averaged fields will help to interpret such variability. Furthermore, several recent papers have pointed out that the Adriatic is undergoing long-term changes in its physical and biogeochemical properties; however, strong inter-annual variability, especially in the surface layers, has, up to now, prevented a consensus on the tendency (Malačič et al., 2006; Mauri et al., 2008; Solidoro et al., 2009; Vilibić et al., 2013). With the overall aim of verifying the stability of the climatology obtained, we focused attention on the deepest parts of the basin, which are regarded as providing the most suitable records of possible long-term changes.

The Adriatic Sea seems to be, at first glance, an ideal candidate for such climatological studies because it has been intensively investigated for more than a century, the first historical oceanographic expeditions dating back to the end of the XIX century (Wolf and Luksch, 1881). During the XX century, a large number of research and monitoring projects have provided a huge amount of data on physical, chemical and biological oceanography. Most papers have, however, addressed a specific area, such as the Northern Adriatic (e.g.: Supić et al., 2004; Jeffries et al., 2007; Tedesco et al., 2007; Giani et al., 2012), the Central Adriatic (e.g. Marini et al., 2006; Russo et al., 2012; Vilibić et al., 2012) and the connection between the South Adriatic and the Ionian Sea (e.g. Klein et al., 2000; Manca et al., 2003, 2006; Civitarese et al., 2010). The most recent climatological description of the Adriatic Sea as a whole dates back to the seminal papers of Artegiani et al. (1997a, b), Gačić et al. (1997) and Zavatarelli et al. (1998), all based on datasets now more than 15 yr old. Therefore, a climatological

OSD
11, 331–390, 2014

study of the whole basin based on recent datasets (up to 2009) is timely and in some sense required.

The overall aim of this study, to provide information on the state of the whole Adriatic Sea and on its variability, is specified in the following objectives:

- to provide an updated climatology for some relevant properties of seawater (temperature, salinity and dissolved oxygen) for the whole Adriatic Sea, starting from a comprehensive dataset spanning a whole century (1911–2009);
- to derive, for each climatological field approximation, an uncertainty map that includes the approximation error, the representativeness error and the experimental error;
- to assess long-term variability in temperature, salinity and dissolved oxygen of the deep waters of the central and Southern Adriatic Sea.

The paper is organized as follows: Sect. 2 presents the physiography of the Adriatic Sea, the description of the datasets used, and the methodology adopted for oceanographic field reconstruction, for method calibration and validation and for long-term variability assessment; Sect. 3 presents the results and the discussion of the climatological maps produced, together with their associated uncertainty and the long-term variability of oceanographic properties of the deep waters; conclusions are then summarized in Sect. 4; further information on the methods of analysis are included in the Appendix and additional plots are available on OGS-NODC web site.

2 Study area, material and methods

2.1 Physiography and climatological circulation features

The Adriatic Sea lies in the northernmost part of the Mediterranean Sea and it is generally approximated as a rectangular basin 800 km long and 200 km wide, where the only connection with the Mediterranean Sea is through the Otranto Strait (72 km wide) (Fig. 1). The basin is characterized by a strong asymmetry along both axes due to increasing depth from the shallow northern basin (average depth 35 m) to the much deeper southern basins (average depth 800 m and deepest pit slightly over 1200 m), and due to the different morphology and bathymetry of the eastern and western coastal areas. In terms of its bathymetry, the Adriatic is generally divided in three sub-basins: (i) the North Adriatic, defined as the area limited by the 100 m isobaths, represents the largest shelf area of the entire Mediterranean and is influenced by the largest river contribution of the whole basin (Cushman-Roisin et al., 2001); (ii) the Middle Adriatic, with a mean depth of about 140 m, extends to the Palagruža Sill (170 m) and includes three adjacent depressions, the Jabuka Pits or Middle Adriatic Pits (MAdP; 255, 270 and 240 m); and (iii) the South Adriatic connects with the Ionian Sea through the Otranto Sill (780 m) and includes the deepest part of the basin, the South Adriatic Pit (SAdP; 1200 m) (Artegiani et al., 1997a).

The general circulation pattern is cyclonic, consisting in the Eastern Adriatic Current (EAC), flowing northwards along the eastern coast with several re-circulation cells steered by bottom topography, and the Western Adriatic Current (WAC), flowing southwards along the Italian shelf. The WAC originates South of the Po River, the main continental input to the Adriatic Sea, and delivers southwards freshwaters as well as suspended and dissolved substances discharged by the rivers along the Italian coast; it is delimited eastwards by a strong haline front. The EAC enters the Adriatic through the Otranto Sill on its eastern side and is composed, in the surface layer, of Ionian Surface Water (ISW) and Modified Atlantic Water (MAW) and, in the intermediate layer, of Modified Levantine Intermediate Water (MLIW). Part of the EAC recirculates along its northward flow, forming several permanent structures (South Adriatic, Middle Adriatic and North Adriatic Gyres), and part of the EAC occasionally reaches the northernmost part of the basin (Poulain, 2001). Because of the significant freshwater river discharge the Adriatic Sea is considered a dilution basin for the whole Mediterranean Sea (Raicich, 1996). The atmospheric forcing, particularly the wind regime, causes an

OSD
11, 331–390, 2014

annual mean heat loss of about 20 W m^{-2} which is, however, subject to significant interannual variability (12 W m^{-2}) due mostly to winter climatic conditions (Cushman-Roisin et al., 2001; Cardin and Gačić, 2003). In the North and in the South Adriatic, the winter heat loss is far more energetic and it can lead to dense water formation (albeit through different physical processes) which eventually also influences the biogeochemical dynamics (Gačić et al., 1997).

Several studies focusing mainly on the northern and central basins have demonstrated large interannual as well as seasonal and shorter term variability in the circulation and in the physical and biogeochemical properties of the upper layer, which is mostly influenced by modifications in meteorological forcing and continental inputs (e.g.: Marini et al., 2006; Jeffries and Lee, 2007; Querin et al., 2007; Boldrin et al., 2009; Lipizer et al., 2011; Mihanovic et al., 2011). The surface layer is thus characterized by pronounced mesoscale variability which responds to the dynamics of the wind regime and of continental discharge (e.g.: Bignami et al., 2007; Cosoli et al., 2012). In the intermediate and deep layers, recurrent variations in the hydrology and biogeochemistry have long been observed in the Southern Adriatic and have been ascribed to the periodic ingression of saltier waters from the Eastern Mediterranean (Buljan, 1953 and subsequent papers) and, more recently, to a bimodal oscillating circulation pattern involving exchanges between the Adriatic and the Ionian Seas (BiOS; Bimodal Oscillating System) on a decadal scale (Borzelli Eusebi et al., 2009; Gačić et al., 2010). The renewal of the deepest part of the Adriatic also depends on the sinking of dense water produced in the northern part of the basin (North Adriatic Dense Water; NAdDW) whose formation rate varies on an interannual time-scale, as a function of winter air–sea fluxes (Manca et al., 2002; Vilibić, 2003). As the deep water outflow from the Adriatic represents a key component for the Ionian and Eastern Mediterranean deep circulation (Ovchinikov et al., 1985), modifications in the properties of deep waters influence the whole Eastern Mediterranean (Roether et al., 1996; Rubino and Hainbucher, 2007; Bensi et al., 2013).

OSD
11, 331–390, 2014

2.2 Dataset

The dataset used in this study includes all data of potential temperature (hereafter named temperature, T, expressed in °C), salinity (S) and dissolved oxygen (DO; $\mathrm{mL\,L^{-1}}$) for the whole Adriatic Sea, from 1911 to 2009 (Fig. 2), available in the Italian National Oceanographic Data Centre (NODC) database managed by OGS (Istituto Nazionale di Oceanografia e di Geofisica Sperimentale). Data have been collected in the framework of several national and international research projects since 1911 by the institutions listed in the Appendix (Table A1). Merging data collected over a century, originating from different sources, acquired by different instruments and with different experimental protocols poses the problems of obtaining a consistent dataset that can be used to provide reliable climatological maps and of long-term data comparability. However, even though intercomparison biases among datasets collected over a century cannot be absolutely ruled out, data managed by NODC undergo internationally standardised Quality Control (QC) procedures (Giorgetti et al., 2005; Holdsworth, 2010; SeaDataNet, 2010) which guarantee the consistency of the merged data: each datum is tagged with a quality flag according to its compliance with QC rules (e.g. out-of-range values, presence of spikes, comparison with mean profiles and their associated standard deviations). The data considered here exhibit "good" or "probably good" QC value flags (1 or 2 following SeaDataNet scale). Furthermore, the problem of pooling a whole century's data, acquired with sensors and techniques with different nominal accuracies, has already been addressed by previous authors (Artegiani et al., 1997a; Zavatarelli et al., 1998), who showed that spatial and temporal variability in physical parameters and in dissolved oxygen concentration largely exceeds any discrepancy introduced by the different accuracies associated with the utilized methods. We paid special attention to exploring the uncertainty due to the field reconstruction method used and due to intrinsic variability of the data which results from the sum of experimental errors and of the natural variability of the different areas.

OSD
11, 331–390, 2014

The climatological field reconstructions were performed on 26 levels, from the sea surface to the bottom, with decreasing vertical resolution. The depth levels correspond to the following depths (in metres): 0, 5, 10, 15, 30, 50, 60, 70, 80, 100, 120, 140, 150, 160, 180, 200, 225, 300, 350, 400, 450, 500, 600, 800, 1000 and 1200. Up to 50 m, the data considered in each level lie within a ±0.5 m layer, increased to ±1.0 from 60 to 180 m, to ±2.5 m from 200 to 800 m and ±10.0 m from 1000 to 1200 m.

To highlight the main structures present in the basin at different depths we present here climatological field reconstructions from the layers at 0, 50, 100 and 200 m; field reconstructions of the other layers are available on OGS-NODC web site.

2.3 Methodology for oceanographic field approximation

The new and updated climatology has been produced with the Variational Inverse Method (VIM; Brasseur et al., 1996), using the software DIVA (Data-Interpolating Variational Analysis; Troupin et al., 2010). DIVA is an appropriate numerical implementation of VIM suitable for this case, as it is designed to perform data-gridding tasks, specifically tailored to accommodate the intrinsic nature of oceanographic data, such as the uncertainty in the in situ measurements, and the irregular coastline and topography (Troupin et al., 2010, 2012). The VIM method obtains the approximated continuous fields reconstruction using a Finite Element Method (FEM), widely used in the oceanographic field to reconstruct variable fields in space (Bretherton et al., 1976; Brasseur et al., 1996). Under specific conditions, the Objective Analysis (OA, Gandin, 1969) has been shown to be equivalent to a VIM analysis (McIntosh, 1990); this analogy constitutes a statistical justification of the variational analysis method and of the evaluation of the relative error maps (Brankart and Brasseur, 1998; Rixen et al., 2000). Conversely, the FEM allows the solution to be determined on an unstructured grid, and this has been proved to be quite effective in many real applications where bathymetries and coastlines are complex, such as the Adriatic basin. This has, moreover, a fundamental advantage over the OA, as the solution is intrinsically found only on the grid elements (which are by definition on the ocean). Hence, the covariance across obstacles or land

OSD
11, 331–390, 2014

is reduced and the anisotropy of the background covariance is "naturally" introduced. Finally, OI implementation must consider all the data at the same time, generating and inverting a covariance matrix of the order of the number of data, while VIM needs to take into account only the number of nodes. For example, the surface temperature measurements are 25 170 over the Adriatic and the basin has been divided into 4500 cells, resulting in a considerable decrease in the computational costs. Using DIVA allows then an efficient reconstruction of values from irregular positions of data points to a regular grid and provides an error map associated with the approximated fields. The methods only requires the definition of two parameters needed to identify a priori the quality of the data (signal-to-noise ratio; SNR) and the statistical spatial structure (correlation length). The parameter selection procedure is described in detail in the Appendix.

The maps produced have a spatial resolution of 1/16° and the GEBCO bathymetry has been used, with 1/60° resolution (https://www.bodc.ac.uk/data/online_delivery/gebco/), to identify the coastlines.

2.4 Validation methodology

All approximation and interpolation methods are based on some idealized assumptions of the underlying statistics that are seldom fully respected by real oceanographic observations, and an evaluation of the approximation process is, therefore, required.

In this study, the validation process is implemented in two steps: Temperature–Salinity (*TS*) diagram comparison and Ordinary Cross Validation.

To verify that the temperature and salinity approximation (carried out independently) does not negatively affect the combined *TS* properties of the water masses, a comparison was made between *T* and *S* charts obtained from the approximated and the in situ data at 100 m depth (summer) and 200 m depth (winter) in order to explore the different behaviour during stratification and deep mixing conditions.

In addition, to validate the field approximation methodology and the robustness of the parameter choice, an Ordinary Cross Validation (OCV; Brankart and Brasseur, 1996)

OSD
11, 331–390, 2014

was performed on the Adriatic dataset: in this case, the seasonal temperature and salinity datasets of the surface and 100 m depth have been used. Ten data subsets were randomly created with 90 % of the original data each. The reconstructed values at the positions of data removed from each data subset were then compared with the measured ones from the whole dataset.

Let us define the set of observations d_m, their relative positions vector $\boldsymbol{t}_m$ (an ordered couple of values that identify latitude and longitude) and the approximation field y_m calculated at the same coordinates:

$$\{d_m\}, \{\boldsymbol{t}_m\}, \{y_m\} \quad 1 \leq m \leq N \tag{1}$$

From these sets we can define K subsets obtained by randomly removing 10 % of the N elements from the observations set:

$$\{d_i^k\}, \{y_i^k\} 1 \leq i \leq L \tag{2}$$

where L is 90 % of the N elements and $1 \leq k \leq K$.

It is worth noting that more than one d_i can be associated to y_i^k (as in the case of oceanographic cruises repeated on the same observational grid).

For each kth subset, the cumulative quadratic observations-approximations misfit V_k is computed as follows, comparing only the data excluded in any kth subset:

$$V_k = \frac{1}{L} \sum_{i=1}^{L} \left(d_i^k - y_i^k\right)^2 \tag{3}$$

The Ordinary Cross Validation V_0 is then defined as:

$$V_0 = \frac{1}{K} \sum_{k=1}^{K} V_k \tag{4}$$

This metric can quantitatively assess the skill of the approximation method in reconstructing the field, but can also help in finding the "best" approximation parameters (Troupin et al., 2012).

OSD
11, 331–390, 2014

2.5 Misfit and qualification of the climatological maps

Let us introduce the sets on indexes N_i whose elements satisfy the condition to share the same position $\boldsymbol{t}_n$

$$N_i \equiv \{j\}\ldots\forall_j : \boldsymbol{t}_j = \boldsymbol{t}_j \text{ with } i \neq j \quad (5)$$

Let's define the Climatology–Observations Misfit (COM) u_i calculated in the ith position of the grid where N_i observations are available as:

$$u_i = \frac{1}{N_i}\sqrt{\sum_{m=1}^{N_i}(d_m - y_i)^2\,\{m = 1,\ldots,N_i\}}$$

where y_i is the value of the approximated field in the ith position, d_m are the original data at the ith position and N_i is the number of in situ data available in the same point. The functional form is quite similar to the OCV but, in this case, COM is applied to all observations. The square-norm data-model misfit is widely used both in the OCV and in data assimilation techniques, and is formally similar to the above-defined quantity; however, the interpretation is different as shown below. COM is here considered a measure of the uncertainty u_i associated with the climatological map.

The use of the observations in different frameworks (the climatology is one paradigmatic case) may introduce synopticity and representativeness errors in the processing of the information that may substantially increase the COM estimate, in particular when historical datasets spanning vast areas and several decades are processed. The seasonal approach in building this climatology is meant to reduce the synopticity error, relying on the hypothesis that the seasonal mode of variability is the dominant one. The noise associated with the ith observation is particularly difficult to appraise as it is derived from the sum of a number of random and deterministic errors (JCGM, 2008), specific to every measurement. The noise is globally retained in the approximation process by selecting a definite signal-to-noise (SNR) ratio used as a weight by DIVA solver

OSD
11, 331–390, 2014

for the minimization of the cost function that forces the piece-wise approximant shape functions to be proximal to the observations. The higher is the SNR, the nearer the approximation (but the more patchy the overall solution).

The misfit produced by approximation solvers is commonly ascribed to the error introduced by the approximation procedure only and, as in case of DIVA, a statistical error estimate e_i comes along with the interpolation procedure. The error estimate e_i is based, as for the Optimal Interpolation, on a stationary, space-invariant covariance function structure which is chosen a priori on the basis of physical intuition and depends on the data coverage only (not on the observation values). In the case of climatology, this simplified hypothesis cannot hold, making this error estimate inappropriate.

Conversely, COM can be representative of real fluctuations in the sea properties that are generated by small-scale dynamics and by interannual variability. This is the case when the approximant function is loosely bound to the data (low SNR) and the combination of the noise associated with the observations with the approximation errors (e_i) are lower than COM itself.

In this case, the uncertainty is informative and can be used to provide additional information on the mesoscale and sub-mesoscale processes active in the region. Unfortunately, rigorous statistical methods can seldom be applied because the a priori information and the statistics of the cumulative uncertainty are largely unknown. In practice, in homogeneous datasets the uncertainty u_i and the approximation errors e_i are expected to be space-invariant and the misfit should depend on the data coverage only (if the approximation parameters are held as constant). In climatological cases, the data are generally abundant and, therefore, the spatial structure of the misfit should exhibit limited variation. If this is not the case, and all the above assumption are still valid, this can be the symptom of an intrinsic variability captured by the observations.

As an example, in the case of recurrent presence of fronts, the temporal distribution of the observations is not unimodal and the approximation cannot represent, at the same time, the most probable conditions. To display the misfit, u, associated with each climatological map, the median misfit was computed for four reference levels (0 m –

50 m – 100 m – 200 m) and for four seasons and expressed as normalized percentage deviation from the value of the approximated field (y_i).

2.6 Determination of long-term variability

Long-term variability in the properties of the deep waters of the Central and South Adriatic was investigated using all data collected during the period 1911–2009 and available in the NODC database (Table A1, Appendix A). For the Central Adriatic, "deep waters" were defined as those below 150 m, in order to limit the effect of seasonal thermocline changes (Artegiani et al., 1997a; Zavatarelli et al., 1998) and in order to focus on the properties of the Jabuka Pits. For the South Adriatic, "deep waters" were defined as those below 800 m, in line with earlier definitions (Zavatarelli et al., 1998), in order to exclude from the analysis the Modified Levantine Intermediate Water (MLIW) which is usually centred around 150–400 m (Zavatarelli et al.,1998; Vilibić and Orlić, 2001).

In order to use a statistically adequate number of data for each sub-basin, the temporal evolution of temperature, salinity and oxygen concentration has been evaluated from median values computed over periods of 5 yr, so filtering out the shorter time scales. The time-series are presented as boxplots showing median, interquartile range (IQR) and min–max range. Finally, temperature and salinity data were used to derive the equilibrium saturation concentration of dissolved oxygen, and the derived variable Apparent Oxygen Utilisation (AOU; $mL\,L^{-1}$) was calculated from the difference between the saturation concentration and the measured dissolved oxygen concentration. Long-term variability in AOU was used in order to allow a better understanding of deep water variability and renewal.

To verify whether differences between median properties characterizing the 5 yr periods were statistically significant, the non-parametric unpaired Mann–Whitney U test (Mann and Whitney, 1947) was used because of the non-normal distribution of data. Statistically significant differences were considered those with p values lower than 0.05. The non-parametric Mann–Kendall (MK) test was used together with Sen's Slope

OSD
11, 331–390, 2014

Estimator for the determination of long-term trend and slope magnitude (Mann, 1945; Sen, 1968; Kendall, 1975). Statistical analysis was performed with Statistica7 StatSoft, XLSTAT software and Kendall–Theil Robust Line V 1.0.1 (Granato, 2006).

3 Results and discussion

3.1 Calibration and validation

Figure 3 shows the comparison between in situ and reconstructed *TS* data from summer at 100 m and winter at 200 m depth. The comparison between in situ and reconstructed *TS* diagrams shows the lower dispersion in the reconstructed fields, owing to the fact that climatology partially filters out the variability, capturing only the "core" of the signal. Both datasets lie largely in the same range of density anomaly, between 28.5 and 29.5 $kg\,m^{-3}$ in summer and between 28.75 and 29.5 $kg\,m^{-3}$ in winter. In summer, densities cluster along the 29.00 $kg\,m^{-3}$ isopycnal, with the exception of the warmest and saltier waters that are less dense (and warmer) than 29.00 $kg\,m^{-3}$. The winter *TS* diagram exhibits the presence of two distinct patterns (more evident in the climatology) connected to the different water masses (MLIW, lighter, warmer and saltier) and MAdDW (denser, colder and fresher) that characterize the thermohaline properties of this level (Artegiani et al., 1997a).

The next step of calibration and validation, based on Ordinary Cross Validation, shows that outputs of OCV (Fig. 4) are reassuringly independent of the spatial distribution, showing a mean misfit between original dataset and each data subset that depends on season and depth but is, in all cases, lower than 0.11 °C for temperature and lower than 0.06 for salinity.

Within each season and level, the misfit of all data subsets lies generally within a narrow interval. This distribution depends on the variability of the spatial structures (larger at the surface), making it sometimes difficult to reconstruct the in situ data and thus increasing the misfit. The variability in the misfit can be also explained taking into

OSD
11, 331–390, 2014

account the selection of the data subsets that do not consider the mutual correlation among data, i.e. all the data are assumed to be uncorrelated. In this way, even if the same number of data points is subtracted in building each data subset, the total available information is not equal. As expected, for both parameters, misfits were larger in the surface level than at 100 m depth, due to the larger space and time variability of the oceanographic fields.

It is worth noting that for temperature (Fig. 4a), winter surface misfits (0.03 °C) are similar to those at 100 m depth, largely due to the vigorous mixing that generally takes place in this season, homogenizing the water column.

Conversely, the salinity (Fig. 4b) shows a stronger difference between the two levels, mostly because the freshwater input signal is limited to the surface.

3.2 Climatological maps

3.2.1 Surface

The surface distribution of temperature, salinity and dissolved oxygen concentration exhibits a strong seasonal cycle (Figs. 5.1–12). A common feature present all over the seasons is the clear signal of the river-diluted WAC, confined along the Italian coast by sharp horizontal gradients (usually stronger in winter and in autumn) and extending as far as the Gargano peninsula. The highest salinities ($S > 38$) characterise the waters flowing along the eastern coasts and occupying the southern and the central basins, and the highest values are observed in winter, particularly in the area of the South Adriatic Gyre (SAdG; Fig. 1). Dissolved oxygen concentration in the surface layer presents a clear seasonal cycle, influenced firstly by water temperature and salinity, gas solubility in seawater being inversely correlated with temperature and salinity, and secondly by biological processes of plankton production and respiration.

Winter is characterised by a pronounced North–South and a less pronounced, but still well recognisable, West–East gradient in surface temperature, with lowest values (7 °C) in the northernmost part of the basin and close to the North-Western Italian

OSD
11, 331–390, 2014

coast. Warmer waters ($T > 13\,^{\circ}$C), typical of the EAC, occupy the eastern part of the basin (Fig. 5.1). The cold waters are formed in the shallow North Adriatic shelf by a wind-driven intense heat loss and a reduced stratification due to a limited freshwater input. The winter cooling in the North Adriatic is a prominent feature of the whole sub-basin. The cold waters' southward pathway is geostrophically confined along the western coast, determining pronounced horizontal gradients which are clearly recognisable even south of the Gargano peninsula. A low-temperature low-salinity patch (Figs. 5.1–5.2) is located along the western coast of the Otranto Strait and this feature is also detectable in the 50 m and 100 m climatology (Fig. 5.13, 5.25). Its origin can be ascribed to intermittent WAC–South Adriatic Gyre interactions and the strong baroclinic characteristics of the WAC. Surface salinity distribution shares some common features with surface temperature, having as the dominant signal the river-diluted WAC ($S < 35$), whose dynamics are, however, density-driven by the low temperature values. In all seasons, but mostly in winter and spring, low salinity waters from the Po River plume also show a north-eastwards propagation, nearly reaching the Eastern Croatian coasts (Fig. 5.2–5.5), suggesting that floods can alter the usual Po plume dynamics. The presence of this (weaker) Po signal off the Italian coast in a long time series suggests that the episodic recurrent flood extreme events are able to influence the climatology. As a remark, it appears that the climatology incorporates both modes of the Po River influence zone, with an intensity roughly proportional to their relative frequency of occurrence.

The absence of large scale mesoscale structures due to the decrease in internal Rossby deformation radius induced by the weak stratification makes the temperature and salinity fields more uniform than in other seasons. On the Northern Italian coast, however, the combined effects of the Po River and of the shallow bathymetry create an evident signal corresponding to an estuary with enhanced cooling of the surface water. This last process is again a consequence of strong Bora events confining the current near the Italian coast. Dissolved oxygen concentration in winter (Fig. 5.3) is tightly related to the physical properties of the surface layer, with the highest oxygen

OSD
11, 331–390, 2014

concentrations (DO > 7.5 mL L^{-1}) associated with the low-salinity waters forming the WAC and observed in the coldest part of the basin (Fig. 5.1).

Spring surface distribution is no longer related only to the WAC system, at least in temperature, and higher values are found over the entire basin. Spatial gradients are much weaker: the warmer EAC ($T > 18\,^{\circ}$C) flowing along the eastern coast and its spreading westwards in the South and Mid-Adriatic Gyres (MAdG) is clearly identified through its temperature signal, and the coldest surface waters ($T = 15\,^{\circ}$C) are found in the Quarner area (Fig. 5.4). As reported by Gačić et al. (1997) from satellite SST data, spring is characterised by inversion of the horizontal temperature gradient, as the coldest waters are present along the eastern coast. Another warm area is observed in the central Adriatic, close to the Jabuka Pits, which may confirm the presence of anticyclonic circulation already proposed by Gačić et al. (1997). In contrast to winter, in spring lower salinity waters ($S < 36$) are distributed over a larger area and tend to occupy a large part of the North Adriatic. As in winter, the low-salinity Po River plume shows a north-eastward propagation up to the Eastern Croatian coasts (Fig. 5.5). In the South Adriatic, a salinity decrease is also well recognisable close to the Albanian coast, indicating the effect of freshwater discharge. Seasonal heating drives an overall decrease in the surface oxygen concentration due to the lower gas solubility in warmer waters; North–South and West–East gradients are still recognisable, with higher oxygen concentrations (DO > 6. 5 mL L^{-1}) in the northern and western regions of the Adriatic, close to the Po River mouth and to rivers in the northernmost part of the basin (Fig. 5.6). In these areas, rich in nutrients from the river loads, increased oxygen can be a consequence of enhanced primary production, which is usually particularly intense South of the Po River (Mauri et al., 2007).

During summer, waters of Ionian origin flowing along the eastern coast are slightly colder (23 $^{\circ}$C) than the rest of Adriatic surface waters and the coldest waters are present in the Quarner and Dalmatian islands areas (Fig. 5.7). The WAC is not recognised either in spring or in summer from the temperature field, while in both seasons lower-salinity waters ($S < 36$) are distributed over a wide area and tend to occupy a large part of the North Adriatic (Fig. 5.8). This distribution probably derives from the wind-driven vorticity input which creates a double gyre system that, together with the strong stratification, facilitates the entrainment of Po River waters in the northernmost part of the sub-basin (Poulain, 2001; Jeffries and Lee, 2007). Dissolved oxygen concentration has furthermore decreased compared to spring (DO mostly $< 6.0\,\mathrm{mL\,L^{-1}}$) and the distribution is fairly uniform, with higher values close to the coast (Fig. 5.9).

Autumn is characterised by the clear signal of the cold WAC ($T < 16\,^{\circ}\mathrm{C}$), confined along the western coast, past the Gargano peninsula and reaching the centre of the South Adriatic, and by the warmer EAC ($T > 18\,^{\circ}\mathrm{C}$) along the south-eastern coasts (Fig. 5.10). Cooling has affected the whole northern, shallower part of the basin ($T < 17\,^{\circ}\mathrm{C}$). The salinity distribution indicates that, in autumn, lower salinity waters are confined as a narrow strip along the coast (Fig. 5.11) and are also characterised by high oxygen concentration (DO $> 6.0\,\mathrm{mL\,L^{-1}}$) (Fig. 5.12).

The overall pattern of the surface distribution of physical properties agrees with the earlier climatology of Artegiani et al. (1997b), Zavatarelli et al. (1998) and Russo et al. (2012). However, comparing the climatological seasonal properties of the Adriatic Surface Water provided by Zavatarelli et al. (1998), based on a narrower time range (1911–1991) and on a coarser spatial resolution, especially in the Mid and South Adriatic, it is remarkable that our climatology, which includes almost two more decades (1991–2009), provides higher temperatures (up to $+2\,^{\circ}\mathrm{C}$) over the whole basin in spring, summer and, in the case of the northern and the southern part of the Adriatic, also in autumn.

Finally, the comparisons between satellite SST climatology (Marullo et al., 2007; SeaDataNet Climatologies, 2011) and climatological maps based on in situ data gave consistent results in all seasons as the principal patterns (e.g. latitudinal and longitudinal thermal gradients) are well revealed by both products.

OSD
11, 331–390, 2014

3.2.2 50 m depth

The 50 m depth layer is characterised, in all seasons, by remarkable differences between the Northern and the Southern Adriatic.

In winter, cold waters fill the North Adriatic and the 100 m isobaths, delimiting the North Adriatic (Fig. 1), seem to limit the northwards propagation of the warmer EAC, resulting in a marked North–South temperature gradient (Fig. 5.13). The strong temperature gradient present in correspondence with the deepening of the bottom may result from the sinking of the cold (thus denser) waters of the North Adriatic shelf below the warmer waters of the central basin, so forming a strong thermal front. Lower salinity waters occupy the margins of the basin and the lowest salinities characterise the western part of the Otranto Strait (lowest salinity core < 38.30) (Fig. 5.14). Conversely, the South Adriatic Pit is characterised by high salinity ($S > 38.6$) and by a temperature relative minimum ($T < 13.5$). Dissolved oxygen presents a limited area of low concentration in the northern part of the shelf (DO $< 5.5\,\mathrm{mL\,L^{-1}}$), southward of the Po River outflow, owing to the combined effect of oxidation of the large loads of organic matter delivered by the river and of the strong and permanent haline stratification which limits ventilation of the bottom layer (Artegiani et al., 1997b; Russo et al., 2012). The South Adriatic Pit exhibits a prominent oxygen minimum (DO $< 5.3\,\mathrm{mL\,L^{-1}}$) coincident with salinity and temperature relative extremes (Fig. 5.15). This feature is most probably produced by the winter-intensified cyclonic circulation that induces the uplifting of deeper and oxygen-depleted waters. In spring, the temperature distribution (Fig. 5.16) and, to some extent, also the overall salinity pattern (Fig. 5.17) remain unchanged, apart from the salinity decrease observed along the coast in the northern part and close to Albanian coast. Dissolved oxygen distribution in spring (Fig. 5.18) presents, as in winter, a strong North–South gradient and reduced concentration close to the Po River mouth ($< 5.6\,\mathrm{mL\,L^{-1}}$) and inside the SAdG ($< 5.5\,\mathrm{mL\,L^{-1}}$). From winter to spring and, to some extent, also from summer to autumn, oxygen concentration shows an increase which is characteristic of the whole Adriatic, despite the seasonal warming

OSD
11, 331–390, 2014

which decreases gas solubility. This overall increase in the 50-m-depth layer is the result of phytoplankton productivity. In fact, seasonal thermohaline stratification prevents the sub-surface layer gas exchange with the atmosphere, and oxygen released as a by-product of photosynthesis can accumulate, thus developing the subsurface oxygen maximum which is typically observed at this depth (Artegiani et al., 1997a; Zavatarelli et al., 1998). Despite the general increase in the concentration, the extension of the low oxygen area close to the Po River mouth increases with the progress of the season, reaching its maximum in summer when both thermohaline stratification and microbial respiration processes are highest (Zavatarelli et al., 1998; Celussi and Del Negro, 2012).

In summer, colder waters ($T < 14.0\,^{\circ}$C) are confined in the northern part of the Adriatic Sea and a warmer water intrusion ($T > 15.0\,^{\circ}$C) is evident in the central area (Fig. 5.19). The salinity distribution remains similar to spring (Fig. 5.20), while oxygen distribution presents a different spatial pattern (Fig. 5.21). The low DO concentration water ($\mathrm{DO} < 5.7\,\mathrm{mL\,L^{-1}}$), always present along the north-western coast, occupies a wide part of the northern shelf almost reaching the eastern coast. Low oxygen concentrations also characterise the margins of the South Adriatic and a slightly lower concentration is still recognised inside the SAdG.

In autumn, cooling has affected the whole basin and the northward propagation of the EAC is the dominant feature recognizable by its warmer temperature ($T > 17\,^{\circ}$C) (Fig. 5.22). The salinity pattern resembles the winter distribution, with lower salinity encountered along the western coast as far as the Otranto Strait (Fig. 5.23). Dissolved oxygen displays lower concentrations in the North, and along the coasts, both on the western side and in some areas along the eastern coasts, as observed in summer (Fig. 5.24). The abovementioned SAdG impact on the water properties is again clearly detectable.

OSD
11, 331–390, 2014

3.2.3 100 m depth

In the 100 m layer, the temperature and salinity show limited seasonal variability (Fig. 5.25–5.36). Dissolved oxygen concentration presents a general decrease from spring to summer, when the lowest concentrations are observed (Fig. 5.33), indicating the prevailing effect of microbial mineralization processes in this layer. Hydrological properties and dissolved oxygen concentrations of the central and the Southern Adriatic are clearly different. The central basin is occupied by colder, fresher and oxygen-richer waters originating in the Northern Adriatic. Bathymetry seems, thus, to act as barriers limiting exchanges between the two basins: the SAdG signature is stronger in autumn and winter and the intensified cyclonic circulation traps the waters entering the Otranto Strait in a recirculation that homogenizes its properties. In spring, summer and autumn the central Adriatic presents a longitudinal thermal and salinity gradient which is due to spreading of the MLIW, recognised by the saltier, warmer and low-oxygen waters ($T > 13.5\,^{\circ}$C, $S > 38.6$, DO $< 5.2\,\mathrm{mL\,L^{-1}}$) protruding along the eastern flank of the basin and crossing the Palagruža Sill. In autumn, temperature (Fig. 5.34), salinity (Fig. 5.35) and oxygen distribution (Fig. 5.36) resemble the winter pattern, with a clear separation of the colder, fresher and oxygen-richer waters in the central basin and the pool of relatively colder, saltier and oxygen-poorer waters confined inside the SAdG.

3.2.4 200 m depth

The 200 m climatology includes only the Mid and the South Adriatic Pits, which are physically separated by the shallow (170 m) Palagruža Sill. At 200 m, seasonal variability is hardly recognizable but the spring climatological maps (Fig. 5.37–39) show clear differences between the properties of the Mid Adriatic and the South Adriatic waters. During all seasons (see Appendix B), the two deep basins are characterised by significant differences in temperature, salinity and oxygen concentration, the Mid Adriatic Pit being characterised by colder ($T < 12.5\,^{\circ}$C), fresher ($S < 38.55$) and, only in spring and autumn, less-oxygenated waters (DO $< 5.1\,\mathrm{mL\,L^{-1}}$), in comparison with the waters at the same depth layer in the South Adriatic ($T > 13.5\,^{\circ}$C; $S > 38.65$; DO $> 5.1\,\mathrm{mL\,L^{-1}}$). The well-known recurrent spill-over of the MAdDW into the Southern Adriatic cannot be detected in this layer because the incoming waters are significantly denser than the SAdG ambient water. Furthermore, because of the episodic periodicity their signatures are difficult to detect in the climatology.

The properties in the deepest parts of the Adriatic are discussed in more detail in Sect. 3.4 and climatological maps of the other layers are available on OGS-NODC web site.

3.3 Average climatology–observation misfits

The seasonal variability in the average COM (u), for each depth layer presented above (Fig. 5), is summarized in Table 1, which shows the median, expressed as a percentage, and the 95th percentile of the COM distribution for the three parameters (temperature, salinity and oxygen) in the four seasons. The 95th percentile has been chosen to provide a spread indicator of the misfit. Table 1 shows that the surface layer exhibits the highest COM, in both temperature and salinity, and that this is greatest in spring for temperature and in summer for salinity. This can be ascribed to the high variability in the forcing fields (wind events, river run-off and related plume dynamics, etc.) influencing mostly the upper layer during the stratified seasons. The surface DO presents an almost constant COM; however, very high 95th percentiles (all exceeding 26.3 %) are found. This may be due to the temperature- and salinity-dependent solubility, to the different sampling techniques adopted over time and to the relative paucity of data if compared with T and S.

COM in the sub-surface layers shows a limited seasonal variability for temperature with a peak autumn 95th percentile below 12.3 % at 50 m and 8.3 % at 100 m. COM in salinity is low (< 0.5 %) and constant throughout the year, with the maximum 95th percentile in all seasons always below 1.0 % in all layers. COM associated with dissolved oxygen climatology in sub-surface layers is higher (median up to 18.5 % at 200 m in autumn) and can reach the highest 95th percentiles in spring and autumn (over 50 % in all layers). This result implies that the interpretation of the DO climatology in the deeper layers must be carried out with some caution and that, in the worst case, the misfit can exceed 51 %.

Considering the spatial distribution of the uncertainty (Fig. 6), it is remarkable that during winter the surface temperature uncertainty (Fig. 6a) exhibits a different distribution with respect to salinity at the same depth (Fig. 6b): salinity uncertainty is highest (up to 30 %) in the north-western part of the Adriatic Sea, influenced by the freshwater input from the Po River. The salinity uncertainty pattern shows a pronounced tongue extending from the Po River mouth towards the centre of the North Adriatic, and the higher u indicates an area of large variability in the offshore freshwater penetration. This area has been, in fact, demonstrated to be very sensitive to prevailing wind regimes and river forcing which can drive the spreading of the Po River plume in opposite directions (Jeffries and Lee, 2007). In this case, the uncertainty map provides clear and additional information on the modes of circulation in the North Adriatic. Temperature uncertainty shows a more uniform spatial distribution and a latitudinal gradient, with higher u in the North Adriatic: this can be related to the stronger impact and to the erratic behaviour of energetic atmospheric forcing such as the Bora winds (strong north-eastern katabatic winds) responsible for intense winter cooling. Contrary to the intuitive belief that more data density will end up in a better statistical estimate, Fig. 6a and b show that the area of maximum data density is associated with the maximum uncertainty, probably because in this area the data distribution is far from being Gaussian, and in the climatology we find a superposition of different, temporally disjoint, patterns. Conversely, the relative approximation error field e (Fig. 6d and e) is at minimum in the Northern Adriatic, as this is dependent only on the data density and not on its values. This means that the uncertainty is representative of an actual site-specific variability which, by definition, the climatology itself is unable to represent.

During summer, the surface temperature uncertainty (Fig. 7a) is lower than in winter and more uniformly distributed along the whole basin; conversely, the salinity

OSD
11, 331–390, 2014

uncertainty is more pronounced in a narrow coastal zone, stronger in proximity to the major river mouths (Fig. 7b). The characteristic tongue observed in winter (Fig. 6b) is no longer recognisable in summer, probably due to the weaker wind regime, to the lower continental inputs and to the spreading of the lighter freshwaters over the entire northern basin, typical of stratified conditions (Jeffries and Lee, 2007). The same consideration on the approximation error fields valid for winter still holds for summer (Fig. 7d and e).

Dissolved oxygen uncertainty at the surface does not reveal any clear spatial distribution, unlike for temperature and salinity; even though, as in the cases of T and S, the North Adriatic is characterized by relatively higher uncertainty, high values (up to 40–70 %) are also calculated in the South, especially in winter (Fig. 6c). Due to the dependence of oxygen solubility on temperature and (to a lesser extent) to salinity, the expected oxygen uncertainty should follow the temperature. This is weakly recognised in winter (Fig. 6a, 6c), when high uncertainty is found in the North and in the South Adriatic; however, in the case of DO uncertainty, several outliers are apparently distributed randomly all along the basin in winter (Fig. 6c) and summer (Fig. 7c). This discrepancy and the relatively high uncertainty can be ascribed to larger experimental errors in sampling and analytical determination of surface oxygen concentration, due to sea–air interactions, than in temperature and salinity. Considered that half of the measurements are below 7 % uncertainty (Table 1), the outcomes of the approximation (climatological maps) are robust enough for climatological purposes. Finally, the approximation error patterns for the two seasons (Figs. 6f and 7f) are not far from those obtained for T and S in both seasons (Figs. 6d, e and 7d, e) with some exception for the coastal areas not covered by observations, which further indicates the prevalent dependence of e on data density.

Comparing the uncertainty (Figs. 6a–c and 7a–c) and error field maps (Figs. 6d–f and 7d–f) it is possible to evaluate the validity of the climatology map. The error field map indicates that, where the number of data is low, the error field is high and the

OSD
11, 331–390, 2014

reliability of the approximation is low. Conversely, the uncertainty map shows how the algorithms used for interpolation mask the natural variability of the data.

3.4 Multi-year trends in the deep waters on a century-scale

Climatologies, by their very nature, tend to smear out any potential temporal trend (the hypothesis of stationarity, at least on the seasonal level, is implicitly assumed as granted). A climatology of a certain variable is informative if the approximated field represents a space-dependent "average" (in a broad sense). This implies that the COM statistical properties should be valid for the whole time spanned by the climatology. In the presence of trends, obviously this is no longer true.

The climatologies presented here have been examined under this perspective on a centennial scale, to identify whether clear temporal trends can be found. In surface waters, the high variability introduced by coastal processes (as testified by the COM analysis reported in Table 1) and the far-from-optimal data coverage (at least for some decades) prevent any sensible trend estimate.

Conversely, the above COM analysis indicates that the uncertainty tends to decrease with depth (Table 1), giving the chance that, below the upper layer, strongly influenced by the seasonal cycle, the relatively small anomalies in specific "hot spots" (Mid and South Adriatic Pits) can be relevant for climatic studies. For the Adriatic, the T, S and DO in the deepest part of the SAdG (< 800 m) are commonly considered as both indicators and drivers of long-term deep ocean processes involving not only the Adriatic Sea but also the whole Eastern Mediterranean.

The dataset used to estimate this climatology spans more than one century, thus enabling capture of signals of climatic variability (if any).

Long-term variability of temperature, salinity, oxygen concentration and AOU in deep waters of the Mid Adriatic and of the South Adriatic Pits are presented in Figs. 8 and 9 as box plots showing the properties in the waters below 150 m in the central Adriatic and below 800 m in the South. The five-year non-parametric statistics are aimed at filtering out the short-term interannual variability identified for both areas (e.g. Marini et al., 2006; Cardin et al., 2011). Most of the medians lie within the range reported by Zavatarelli et al. (1998) for the deep waters in the Middle and the South Adriatic, considering a smaller dataset ending in the early 1990s, and our results are also coherent with inter-annual variability studies based on more recent data (e.g. Marini et al., 2006; Cardin et al., 2011; Vilibić et al., 2011). In addition, this longer time series enables, for the first time, an appraisal of the centennial scale variability.

In the shallower Mid Adriatic Pits, temporal variability between the statistics calculated over consecutive 5 yr periods is pronounced for temperature, with the lowest median in the early 1950s (10.89 °C) and the highest in the early 1960s (12.80 °C) (Fig. 8a). The outcomes of the Mann–Whitney *U* test analysis indicate that median temperatures between consecutive 5 yr periods were in most cases statistically significantly different (10 cases out of 12). An evident rise in deep water temperature is observed in the early 1960s (+1.64 °C compared with the previous period) and late 1990s (+0.89 °C), and a considerable decrease is reported in the first years of the 1980s (−0.63 °C) and in the late 2000s (−0.81 °C). This time-series analysis leads to the conclusion that the dominant mode of temperature variability has a multidecadal scale. In the case of salinity, variability between subsequent 5 yr periods is, in most cases, masked by overlapping IQR (Fig. 8b). The lowest median salinity (38.33) is reported in the first period (1910–1914) and the highest in the late 1970s (38.56). Median dissolved oxygen concentration presents data dispersion which masks variability between subsequent periods, and differences were statistically significant in a limited number of cases (5 out of 11) (Fig. 8c). As an overall tendency, a decrease is recognisable starting from the early 1980s, with the lowest median in the early 1990s (4.2 $mL L^{-1}$), which is, however, calculated from data collected in a single year (1990) and the highest median DO is reported at the beginning of the XX century (5.4 $mL L^{-1}$). Interannual and multidecadal variability in the deep water properties has also been recognised from independent data collected in the Palagruža Sill area. This variability has been ascribed to advection of waters of different origin, due to reversal in the Ionian Sea circulation, and weakening of the thermohaline circulation in the Adriatic (Vilibić et al., 2012, 2013). In

OSD
11, 331–390, 2014

the Mid Adriatic Pits, northwards of the sill, deep water variability can thus have an advective origin both from the South (alternation between ingression of MAW and MLIW) and from the North (fluctuating contribution from NAdDW), as well as a local origin due to in situ ageing. The temporal evolution of apparent oxygen utilization (AOU) was calculated to investigate whether modifications in the oxygen content are due to advection of a different water mass, with its distinctive oxygen concentration, or to local "ageing" consequent on reduced ventilation. Positive AOU indicates the prevalence of microbial oxygen consumption over oxygen replenishment from the upper layers and increasing AOU is, thus, regarded as a proxy for deep-water ageing. In the deep Central Adriatic, median AOU ranges between 0.4 $mL L^{-1}$ in the early 1960s to 1.3 $mL L^{-1}$ in the late 2000s, with large and overlapping IQR in some periods (Fig. 8d). Large variability within each 5 yr period, especially in the case of dissolved oxygen and AOU, is probably related to short-term variability in the hydrological properties of the Mid Adriatic pits due to the periodical, though occasional, renewal consequent on dense water formation over the North Adriatic shelf (Vilibić, 2003; Marini et al., 2006). In particular, the large IQR in the late 1990s reflects the very large variability in dissolved oxygen saturation reported by Marini et al. (2006). Even though differences between consecutive 5 yr periods are statistically significant only in 5 out of 10 cases, since the beginning of this time-series, and mostly since the late 1970s, Sen's trend analysis based on annual median data indicates that apparent oxygen utilization in the deep waters of the Central Adriatic has been continuously increasing (+0.02 $mL L^{-1} yr^{-1}$), possibly indicating a less efficient or frequent ventilation of the deep waters, due to weakening of the surface thermohaline cell as recently proposed by Vilibić et al. (2012, 2013), based on time-series in the Palagruža Sill.

In comparison with the shallower pits of the central basin, in the deep waters of the South Adriatic (> 800 m), data variability within each 5 yr period is reduced (Fig. 9a–d) as indicated by the narrow IQR for all parameters. Variability between consecutive periods is particularly relevant in the case of temperature and salinity. In the case of temperature, differences between subsequent periods are in most cases (8 out of 10) highly

OSD
11, 331–390, 2014
Qualified climatologies in a changing Adriatic Sea
M. Lipizer et al.

statistically significant ($p < 0.01$). The lowest median temperature was measured at the beginning of the time series (12.65 °C) and the highest in the late 1970s (13.23 °C). The early 1980s were characterised, as observed in the MAdP (Fig. 8a), by a significant T decrease (−0.16 °C), as previously documented by Vilibić and Orlić (2001), and by a salinity and oxygen increase, associated with the lowest AOU of the time-series, which suggests an energetic deep water renewal. The end of this time-series was also characterised by a significant T increase in comparison with the late 1990s (+0.27 °C) (Fig. 9a). Salinity presents an overall increase throughout the time-series, with the lowest median in the 1940s (38.51) and the highest in the 2005–2009 period (38.73) (Fig. 9b). Large variability has been observed especially in the late 1960s and 1980s. Median salinity presents an evident rise in the 1970s, concomitant with the higher temperature decade (Fig. 9a and b). Fluctuations on a decadal scale can be detected, possibly connected with the "Adriatic ingression", documented since the XIX century (Buljan, 1953). This periodic variability has been related to reversal in the circulation of the intermediate layers in the Ionian Sea (Gačić et al., 2010) and, for the 1990s, to the influence of the Eastern Mediterranean Transient (EMT) in the Adriatic (Manca et al., 2006; Cardin et al., 2011).

Median oxygen concentrations present pronounced temporal variability, ranging between 5.3 $\mathrm{mL\,L^{-1}}$ during the early 1980s and 4.5 $\mathrm{mL\,L^{-1}}$ in the late 1990s, with particularly pronounced variations in the 1960s and starting from the early 1980s (Fig. 9c). The late 1990s present a dramatic decrease which distinguishes this period from the whole time-series. This period is also characterised by the highest AOU (1.3 $\mathrm{mL\,L^{-1}}$), suggesting significant ageing of the deep waters since the early 1980s (Fig. 9d). The dramatic oxygen decrease, and accompanying AOU increase, associated with significant salinity and limited temperature decrease observed in the late 1990 is a clear sign of reduced deep ventilation consequent on the EMT, which caused the intrusion into the Adriatic of the less saline "old" Eastern Mediterranean Deep Water (EMDW) (Manca et al., 2003). The maximum dilution, i.e. salinty decrease, observed in 1995 had a negative impact on convective processes and deep-water renewal (Cardin et al., 2011),

OSD
11, 331–390, 2014

and brought about the largest AOU of the time-series. This long time series reveals the EMT as the most dramatic "suppressor" of deep water renewal on a century scale, as no other comparable events have been recorded.

Considering together the time scales of temperature, salinity, dissolved oxygen and AOU and the available information on past dense water formation events, one can trace back the ventilation history of the South Adriatic Pit. The lowest AOU in the early 1980s, associated with highest oxygen, relative decrease in temperature and increase in salinity in comparison with the previous period (Fig. 9a–d), all point towards the deep ventilation of the South Adriatic Pit documented in 1982 (Ovchinikov et al., 1985). On the other hand, the abrupt oxygen decrease and AOU increase evident in the early 1960s, characterised by a relative temperature increase and salinity decrease, may indicate that a period of reduced deep ventilation, similar to that consequent to the EMT but much weaker, may have already occurred.

Finally, the last period of this time-series (2005–2009) is characterised by an increased MLIW inflow (high temperature and salinity) and by a concurrent oxygen increase of 0.65 $\mathrm{mL\,L^{-1}}$ since the previous period, which is similar to what occurred between 1999 and 2002 after a new deep ventilation episode (Manca et al., 2006). These properties point towards a recovery of energetic deep-water renewal conditions, which restore pre-EMT oxygen concentration. Conversely, after the effect of the EMT, temperature and salinity of the Adriatic Pit now differ profoundly from the characteristics of the Adriatic Deep Water (AdDW) previously observed, being now warmer and saltier than in the past.

The time series in the Mid and South Adriatic Pits seem mostly characterised by different temporal patterns of variability. Sen's trend estimates calculated in both areas indicate differences between the two areas. The Mid Adriatic Pits (MAdP) show a statistically significant ($p < 0.05$) increasing AOU (+0.2 $\mathrm{mL\,L^{-1}\,decade^{-1}}$) and decreasing trend in DO (–0.1 $\mathrm{mL\,L^{-1}\,decade^{-1}}$) since the late 1970s, while no clear trends are recognisable for temperature and salinity; however, the 1910–1914 salinity data are significantly lower than all the following five-year available periods. This result points

Discussion Paper | Discussion Paper | Discussion Paper | Discussion Paper |

OSD

11, 331–390, 2014

towards the large influence of biogeochemical processes consuming oxygen, which is not efficiently restored by physical processes of dense water formation. Conversely, in the South Adriatic, a statistically robust long-term salinity (+0.018 decade^{-1}) increase is evident, while no trends are evident in DO and AOU variability and, even after the dramatic decline of deep ventilation in the 1990s, physical processes, i.e. open ocean convection, are strong enough to restore deep oxygen concentrations. This can lead to the conclusion that the biotic activity is dominant in the MAdP while physical processes are ruling the biogeochemical properties in SAdP.

Any attempt to directly connect the observed patterns (Figs. 8 and 9) to the well-known decadal climate variability in the Mediterranean region (Mariotti and Dell'Aquila, 2012) turned out to be unsuccessful, suggesting that the complex interactions between physical forcing, internal dynamics and remote control cannot be disentangled by just simple statistical analysis.

4 Conclusions

As a final summary, we can draw the following conclusions:

- A new qualified climatology for T, S and DO has been produced and analysed with an extended dataset. In contrast with earlier climatologies (Artegiani et al., 1997b; Zavatarelli et al., 1998; Russo et al., 2012), the climatology presented in this paper includes data spanning over almost a century (1911–2009) for the whole basin, provides estimates of uncertainty of the observed vs. the revealed structures, is developed for 26 levels, has a spatial resolution of 1/16° and focuses on the deepest parts of the basin.

- The innovative FEM-based DIVA solver has been used in the Adriatic Sea and turned out to be very effective in following the complex coastline that characterizes this basin.

OSD
11, 331–390, 2014

- The qualification of the maps has been achieved using cal/val techniques (Ordinary Cross Validation) and real vs. synthetic *TS* diagram intercomparisons. Misfits calculated from OCV were always less than 0.11 °C for temperature and 0.06 for salinity.

- The concept of data-approximation misfit associated with a climatology has been introduced here, showing its potential to carry additional information. High misfit associated with front space-time variabilities has been detected and it was found to be largest in the surface layer, in spring for temperature (median uncertainty 14.9 %) and in summer for salinity (median 2.1 %). Conversely, dissolved oxygen exhibits higher uncertainty in the deeper layers (median up to 18.5 % at 200 m depth). The Climatology–Observations Misfit analysis can provide important additional information that can be extracted as a by-product of the climatological approximation procedure.

- While the climatological maps confirm the overall picture of the thermohaline properties and of DO for the Adriatic and the prominent seasonal signal connected to the Po River input, additional new features have been identified and described with better accuracy. The surface temperatures are higher (up to 2 °C) than those recorded by Zavatarelli et al. (1998) over the whole basin in spring, summer and, in the case of the northern and the southern part of the Adriatic, also in autumn. In the intermediate and deep layers, a clear DO minimum is typically recognized in the centre of the SAdG due to the doming induced by cyclonic circulation. Conversely, in the North Adriatic the summer DO bottom minimum is driven by biotic respiration processes fuelled by the seasonal loading of nutrient and organic matter discharged by the Po River. Below 100 m, all properties show a limited seasonal variability but are profoundly different between the Middle and the South Adriatic. This indicates that North–South exchanges are limited to the surface layer, where the Region of Freshwater Influence (ROFI) in correspondence to the Po mouth drives a vigorous thermohaline surface circulation. Conversely,

OSD
11, 331–390, 2014

Qualified climatologies in a changing Adriatic Sea

M. Lipizer et al.

the exchanges between the two sub-basins in the intermediate layers appear to be much weaker and possibly limited by the strong topographically controlled recirculation in the SAdG.

- The properties of South Adriatic Pit clearly show the remote effects of EMT (lower salinity, temperature and DO) while no effect is observed in MAdP. The EMT is recognised as the most dramatic signal ever recorded over the whole dataset. This long time series revealed a similar, but less energetic, concomitant variation in T, S and DO in the 1960s. This can lead to the speculation that a weaker EMT-like event could have previously occurred. Referring to the beginning of the time series, the deepest part of the South Adriatic seems now to be significantly saltier (+0.18 since the period 1910–1914, with an increase of +0.018 decade^{-1} since 1945) and also warmer (+0.54 °C since 1910–1914), even though a long-term temperature trend could not be statistically demonstrated. Conversely, the MAdP presents a long-term increase in apparent oxygen utilisation (+0.77 mL L^{-1} since 1910–1914, with a constant increase of +0.2 mL L^{-1} decade^{-1} after the 1970s).

As an overall comment, despite its limited geographical dimensions the Adriatic Sea hosts different interacting processes, sensitive to seasonal and longer term variability. The behaviour differs between its sub-basins and even the deepest pits (located 260 km apart), supposedly prone to reacting similarly to the climatic signal, exhibit different responses. Our reanalysis of data collected since the beginning of the XX century confirms features reported previously by several authors and based on shorter time-windows (Artegiani et al., 1997a; Vilibić et Orlić, 2001; Manca et al., 2003; Cardin et al., 2011; Vilibić et al., 2011, 2012, 2013) but allows, for the first time, appreciation of the importance of phenomena in a century-long perspective and, furthermore, allows the identification of events not yet reported, such as the significant deep ventilation of the SAdP in the early 1980s and a weak EMT-like event probably occurring in the early 1960s.

OSD
11, 331–390, 2014

This climatology can help to define a baseline for the XX century but, at the same time, shows that the more recent data seem to have a different behaviour, with a stronger rate of variability. An apparent speed-up in temperature increase in the SAdP is suggested by the last decade's data and, in light of on-going global changes, deserves specific future investigations.

Appendix A

Mathematical background

The DIVA (Data-Interpolating Variational Analysis) software is designed to solve 2-D variational problems of elliptic type with a finite element method (Troupin et al., 2012).

The field ϕ is that one that will minimize the cost function $J(\phi)$ defined as (Troupin et al., 2010):

$$J[\phi] = \sum_{i=1}^{Nd} \mu_i L^2 (d_i - \phi(x_i, y_i))^2 + \int_D (\nabla\nabla\phi : \nabla\nabla\phi + \alpha_1 L^2 \nabla\phi \cdot \nabla\phi + \alpha_0 L^4 \phi^2)\, \mathrm{d}D \qquad (A1)$$

where d_i are the original data, $\nabla\nabla\phi$: $\nabla\nabla\phi$ is the squared Laplacian of the field ϕ, D is the domain and where additional weights are included to balance the relative contribution of:

- α_0, which penalizes the field itself (anomalies minimization),
- α_1, which penalizes gradients (trends minimization),
- α_2, which penalizes variability (regularization),
- μ, which penalizes data-approximation misfits (objective).

Minimization of Eq. (A1) is actually performed by a Finite-Element Method (FEM), hence the need for generating a finite-element grid. The correlation length (L) is the parameter that defines the dimensions of the grid: every grid element is the combination of three sub-elements. To avoid sub-sampling, it is required that L/3 is smaller than the scale of the dominant processes analysed. In this work, the external parameters "correlation length" (L) and "signal-to-noise ratio" (SNR) have been chosen considering the targets of the specific study. The evaluation of their values directly from statistical properties of the dataset turned out to be impossible due to inhomogeneous spatial and temporal distribution of data. A detailed analysis of the best parametrization has been carried out through an optimization procedure (Generalized Cross-validation) and by testing numerous parameter estimates. The automatic optimization procedure turned out to severely underestimate L as the uneven distribution of the data, often strongly correlated and clustered, led to values close to 0.1°. This L value would introduce spurious high-wavenumber structures dependent only on the data spatial distribution. Eventually, the selected value ($L = 0.8°$ for physical parameters and 1.5° for DO) accounts for the length scale of the long-lasting structures that had to be captured by the climatological analysis. This dimensionless value for the correlation length is coherent with the resolution used in literature for the Adriatic basin (Zavatarelli et al., 1998 and Giorgetti, 1999). We acknowledge the fact that the L value strongly depends on scientific intuition and previous knowledge instead of a statistical algorithm.

The SNR ratio assumed a very low value (0.5), but the "noise", in the case of climatologies, accounts for a number of processes active at different temporal and spatial scales (mesoscale, seasonal cycle, interannual or decadal variability, etc.), thus by far exceeding the simple accuracy and representativeness errors typical of synoptic datasets. The SNR value, thus, is able to accommodate the large (natural) variability reflected in the data distribution around the median. The correlation length and the signal-to-noise ratio are, therefore, directly comparable to the corresponding parameters in OI (Troupin et al., 2012).

OSD
11, 331–390, 2014

The error field associated with the approximated fields has been calculated according to the method based on the real covariance functions, which allows a more accurate estimate of the error (Troupin et al., 2012).

Appendix B

Climatological maps of the levels not presented in the article will be available on OGS-NODC web site after manuscript acceptance.

Acknowledgements. We acknowledge all the institutes and the projects listed in Table A1 (Appendix) for the data used in this research. We also wish to thank B. Manca, V. Cardin, G. Civitarese and V. Kovačević for the more recent data. We acknowledge the GeoHydrodynamics and Environmental Research group (GHER) of the University of Liege, Belgium, for the development of the DIVA analysis software, the support of the Italian flagship project RITMARE and the EU FP6 and FP7 Projects SeaDataNet, SeaDataNet II and EMODNET (MARE/2008/03 – Lot 3 Chemistry) from the Directorate-General for Maritime Affairs and Fisheries.

References

Artegiani, A., Bregant, D., Paschini, E., Pinardi, N., Raicich, F., and Russo, A.: The Adriatic Sea general circulation. Part I: Air–sea interactions and water mass structure, J. Phys. Oceanogr., 27, 1492–1514, 1997a.

Artegiani, A., Bregant, D., Paschini, E., Pinardi, N., Raicich, F., and Russo, A.: The Adriatic Sea general circulation. Part II: Baroclinic circulation structure, J. Phys. Oceanogr., 27, 1515–1532, 1997b.

Bensi, M., Rubino, A., Cardin, V., Hainbucher, D., and Mancero-Mosquera, I.: Structure and variability of the abyssal water masses in the Ionian Sea in the period 2003–2010, J. Geophys. Res.-Oceans, 118, 931–943, 2013.

Bignami, F., Sciarra, R., Carniel, S., and Santoleri, R.: Variability of Adriatic Sea coastal turbid waters from SeaWiFS imagery, J. Geophys. Res.-Oceans, 112, C03S10, doi:10.1029/2006JC003518, 2007.

Boldrin, A., Carniel, S., Giani, M., Marini, M., Aubry, F. B., Campanelli, A., Grilli, F., and Russo, A.: Effects of bora wind on physical and biogeochemical properties of stratified waters in the Northern Adriatic, J. Geophys. Res.-Oceans, 114, C08S92, doi:10.1029/2008JC004837, 2009.

Borzelli, G. L. E., Gačič, M., Cardin, V., and Civitarese, G.: Eastern Mediterranean transient and reversal of the Ionian Sea circulation, Geophys. Res. Lett., 36, L15108, doi:10.1029/2009GL039261, 2009.

Brankart, J. and Brasseur, P.: Optimal analyis of in situ data in the Western Mediterranean using statistic and cross-validation, J. Atmos. Ocean. Tech., 13, 477–491, 1996.

Brankart, J. and Brasseur, P.: The general circulation in the Mediterranean Sea: a climatological approach, J. Marine Syst., 18, 41–70, 1998.

Brasseur, P., Beckers, J. M., Brankart, J. M., and Schoenauen, R.: Seasonal temperature and salinity fields in the Mediterranean Sea: climatological analyses of a historical data set, Deep-Sea Res. Pt. I, 43, 159–192, doi:10.1016/0967-0637(96)00012-X, 1996.

Bretherton, F., Davis, E., and Fandry, C.: A technique for objective analysis and design of applied to MODE-73, Deep-Sea Res., 23, 559–582, 1976.

Buljan, M.: Fluctuations of Salinity in the Adriatic, Reports, II (2). Institut za Oceanografiju i Ribarstvo – Split (Croatia), 64 pp., 1953.

Cardin, V. and Gačić, M.: Long-term heat flux variability and winter convection in the Adriatic Sea, J. Geophys. Res.-Oceans, 108, 4–12, 2003.

Cardin, V., Bensi, M., and Pacciaroni, M.: Variability of water mass properties in the last two decades in the South Adriatic Sea with emphasis on the period 2006–2009, Cont. Shelf Res., 31, 951–965, 2011.

Celussi, M. and Del Negro, P.: Microbial degradation at a shallow coastal site: long-term spectra and rates of exoenzymatic activities in the NE Adriatic Sea, Estuar. Coast. Shelf S., 115, 75–86, 2012.

Civitarese, G., Gačić, M., Lipizer, M., and Eusebi Borzelli, G. L.: On the impact of the Bimodal Oscillating System (BiOS) on the biogeochemistry and biology of the Adriatic and Ionian Seas (Eastern Mediterranean), Biogeosciences, 7, 3987–3997, doi:10.5194/bg-7-3987-2010, 2010.

OSD
11, 331–390, 2014

Cosoli, S., Gačić, M., and Mazzoldi, A.: Surface current variability and wind influence in the Northeastern Adriatic Sea as observed from high-frequency (HF) radar measurements, Cont. Shelf Res., 33, 1–13, 2012.

Cushman-Roisin, B., Gačić, M., Poulain, P., and Artegiani, A.: Physical Oceanography of the Adriatic Sea: Past, Present and Future, edited by: Gandin, L., Kluwer Academic Publisher, Springer, 2001.

European Commission: Water Framework Directive 2000/60/EC, Brussels, Belgium, 2000.

European Commission: Marine Strategy Framework Directive 2008/56/EC, Brussels, Belgium, 2008.

Gačić, M., Marullo, S., Santoler, R., and Bergamasco, A.: Analysis of the seasonal and interannual variability of the sea surface temperature field in the Adriatic Sea from AVHRR data (1984–1992), J. Geophys. Res.-Oceans, 102, 22937–22946, 1997.

Gačić, M., Eusebi Borzelli, G. L., Civitarese, G., Cardin, V., and Yari, S.: Can internal processes sustain reversals of the ocean upper circulation? The Ionian Sea example, Geophys. Res. Lett., 37, L09608. doi:10.1029/2010GL043216, 2010.

Gandin, L. S.: Objective Analysis of Meteorological Fields, Israel Program for Scientific Translations, Jerusalem, 242 pp., 1969.

Giani, M., Djakovac, T., Degobbis, D., Cozzi, S., Solidoro, C., and Umani, S. F.: Recent changes in the marine ecosystems of the Northern Adriatic Sea, Estuar., Coast. Shelf S., 115, 1–13, 2012.

Giorgetti, A.: Climatological analysis of the Adriatic Sea termohaline characteristic, B. Geofis. Teor. Appl., 40, 53–73, 1999.

Giorgetti, A., Burca, M., Manca, B. B., and Tomini, I.: Compilation of a quality-controlled database of biological and chemical oceanographic parameters in the Central Mediterranean Sea, B. Geofis. Teor. Appl., 46, 357–376, 2005.

Granato, G. E.: Kendall–Theil Robust Line (KTRLine-version 1.0) – a visual basic program for calculating and graphing robust nonparametric estimates of linear-regression coefficients between two continuous variables, in: Techniques and Methods of the US Geological Survey, book 4, chap. A7, US Geological Survey, 31 pp., 2006.

Holdsworth, N.: EMODNET Chemical: QC and QA basic guidelines, 10 pp., doi:10.6092/3CB41F4C-C401-45A7-AB32-0ABD373E03BB, available at: http://www.nodc.it/doi/documents/QC_Guidelines_EMD-Chemical_version1.2.doc (last access: 27 November 2013), 2010.

OSD
11, 331–390, 2014

Jeffries, M. A. and Lee, C. M.: A climatology of the Northern Adriatic Sea's response to bora and river forcing, J. Geophys. Res.-Oceans, 112, C03S02, doi:10.1029/2006JC003664, 2007.
JGCM 2008: 100, Evaluation of measurements data – Guide to the expression of uncertainty in measurements, JCGM, 134 pp. available at: http://www.bipm.org/en/publications/guides/gum.html (last access: 27 November 2013), 2008.
Kendall, M. G.: Rank Correlation Methods, 4th edn., Charles Griffin, London, UK, 1975.
Klein, B., Roether, W., Civitarese, G., Gačić, M., Manca, B. B., and d'Alcala, M. R.: Is the Adriatic returning to dominate the production of Eastern Mediterranean Deep Water?, Geophys. Res. Lett., 27, 3377–3380, 2000.
Lipizer, M., Cossarini, G., Falconi, C., Solidoro, S., and Fonda Umani, S.: Impact of different forcing factors on N : P balance in a semi-enclosed bay: the Gulf of Trieste (North Adriatic Sea), Cont. Shelf Res., 31, 1651–1662, doi:10.1016/j.csr.2011.06.004, 2011.
Malačič, V., Celio, M., Èermelj, B., Bussani, A., and Comici, C.: Interannual evolution of seasonal thermohaline properties in the Gulf of Trieste (Northern Adriatic) 1991–2003, J. Geophys. Res.-Oceans, 111, C08009, doi:10.1029/2005JC003267, 2006.
Manca, B. B., Kovačević, V., Gacić, M., and Viezzoli, D.: Dense water formation in the Southern Adriatic Sea and spreading into the Ionian Sea in the period 1997–1999, J. Marine Syst., 33–34, 133–154, 2002.
Manca, B. B., Budillon, G., Scarazzato, P., and Ursella, L.: Evolution of dynamics in the Eastern Mediterranean affecting water mass structures and properties in the Ionian and Adriatic Seas, J. Geophys. Res.-Oceans, 108, 3–19, 2003.
Manca, B. B., Ibello, V., Pacciaroni, M., Scarazzato, P., and Giorgetti, A.: Ventilation of deep waters in the Adriatic and Ionian Seas following changes in thermohaline circulation of the Eastern Mediterranean, Clim. Res., 31, 239–256, 2006.
Mann, H. B.: Non-parametric test against trend, Econometrica, 13, 245–259, 1945.
Mann, H. B. and Whitney, D. R.: On a test of whether one of two random variables is stochastically larger than the other, Ann. Math. Stat., 18, 50–60, doi:10.1214/aoms/1177730491, 1947.
Marini, M., Russo, A., Paschini, E., Grilli, F., and Campanelli, A.: Short-term physical and chemical variations in the bottom water of Middle Adriatic depressions, Clim. Res., 31, 227–237, 2006.
Mariotti, A. and Dell'Aquila, A.: Decadal climate variability in the Mediterranean region: roles of large-scale forcings and regional processes, Clim. Dynam., 5–6, 1129–1145, 2012.

OSD
11, 331–390, 2014

Qualified climatologies in a changing Adriatic Sea

M. Lipizer et al.

Marullo, S., Buongiorno Nardelli, B., Guarracino, M., and Santoleri, R.: Observing the Mediterranean Sea from space: 21 years of Pathfinder-AVHRR sea surface temperatures (1985 to 2005): re-analysis and validation, Ocean Sci., 3, 299–310, doi:10.5194/os-3-299-2007, 2007.
Mauri, E., Poulain, P. M., and Južnič-Zonta, Z.: MODIS chlorophyll variability in the Northern Adriatic Sea and relationship with forcing parameters, J. Geophys Res.-Oceans, 112, C03S11, doi:10.1029/2006JC003545, 2007.
Mauri, E., Poulain, P. M., and Notarstefano, G.: Spatial and temporal variability of the sea surface temperature in the Gulf of Trieste between January 2000 and December 2006, J. Geophys. Res.-Oceans, 113, C10012, doi:10.1029/2007JC004537, 2008.
McIntosh, P. C.: Oceanographic data interpolation: objective analysis and splines, J. Geophys Res., 95, 13529–13541, 1990.
Mihanović, H., Cosoli, S., Vilibić, I., Ivankovi, D., Dadić, V., and Gačić, M.: Surface current patterns in the Northern Adriatic extracted from high-frequency radar data using self-organizing map analysis, J. Geophys. Res.-Oceans, 116, C08033, doi:10.1029/2011JC007104, 2011.
Ovchinnikov, I. M., Zats, V. I., Krivosheya, V. G., and Udodov, A. I.: Formation of deep Eastern Mediterranean water in the Adriatic Sea, Oceanology, 25, 704–707, 1985.
Poulain, P. M.: Adriatic Sea surface circulation as derived from drifter data between 1990 and 1999, J. Marine Syst., 29, 3–32, 2001.
Querin, S., Crise, A., Deponte, D., and Solidoro, C.: Numerical study of the role of wind forcing and freshwater buoyancy input on the circulation in a shallow embayment (Gulf of Trieste, Northern Adriatic Sea), J. Geophys. Res., 112, C03S16, doi:10.1029/2006JC003611, 2007.
Raicich, F.: On the fresh water balance of the Adriatic Sea, J. Marine Syst., 9, 305–319, 1996.
Rixen, M., Beckers, J., Brankart, J., and Brasseur, P.: A numerically efficient data analysis method with error map generation, Ocean Model., 2, 45–60, 2000.
Roether, W., Manca, B. B., Klein, B., Bregant, D., Georgopoulos, D., Beitzel, V., Kovačević, V., and Lucchetta, A.: Recent changes in Eastern Mediterranean deep waters, Science, 271, 333–335, doi:10.1126/science.271.5247.333, 1996.
Rubino, A. and Hainbucher, D.: A large abrupt change in the abyssal water masses of the Eastern Mediterranean, Geophys. Res. Lett., 34, L23607, doi:10.1029/2007GL031737, 2007.
Russo, A., Carniel, S., Sclavo, M., and Krzelj, M.: Climatology of the Northern-Central Adriatic Sea, in: Modern Climatology, edited by: Wang, S.-Y., InTech China, Shangai, China, 177–212, 2012.

OSD
11, 331–390, 2014

Schlitzer, R.: Ocean Data View, available at: http://odv.awi.de (last access: 27 November 2013), 2012.
SeaDataNet Climatologies: available at: http://gher-diva.phys.ulg.ac.be/web-vis/clim.html (last access: 28 October 2013), 2011.
SeaDataNet: Data Quality Control Procedures, version 2.0, 78 pp., available at: http://www.seadatanet.org/Standards-Software/Data-Quality-Control (last access: 27 November 2013), 2010.
Sen, P. K.: Estimates of the regression coefficient based on Kendall's tau, J. Am. Stat. Assoc., 39, 1379–1389, 1968.
Solidoro, C., Bastianini, M., Bandelj, V., Codermatz, R., Cossarini, G., Melaku Canu, D., Ravagnan, E., Salon, S., and Trevisani, S.: Current state, scales of variability, and trends of biogeochemical properties in the Northern Adriatic Sea, J. Geophys. Res.-Oceans, 114, C07S91, doi:10.1029/2008JC004838, 2009.
Supić, N., Grbeć, B., Vilibić, I., and Ivančić, I.: Long-term changes in hydrographic conditions in Northern Adriatic and its relationship to hydrological and atmospheric processes, Ann. Geophys., 22, 733–745, 2004,
http://www.ann-geophys.net/22/733/2004/.
Tedesco, L., Socal, G., Bianchi, F., Acri, F., Veneri, D., and Vichi, M.: NW Adriatic Sea biogeochemical variability in the last 20 years (1986–2005), Biogeosciences, 4, 673–687, doi:10.5194/bg-4-673-2007, 2007.
Troupin, C., Barth, A., Sirjacobs, D., Ouberdous, M., Brankart, J. M., Brasseur, P., Rixen, M., Alvera-Azcárate, A., Belounis, M., Capet, A., Lenartz, F., Toussaint, M. E., and Beckers, J. M.: Generation of analysis and consistent error fields using the Data Interpolating Variational Analysis (DIVA), Ocean Model., 52–53, 90–101, 2012.
Troupin, C., Machín, F., Ouberdous, M., Sirjacobs, D., Barth, A., and Beckers, J. M.: High-resolution climatology of the North-East Atlantic using data-interpolating variational analysis (Diva), J. Geophys. Res., 115, C08005. doi:10.1029/2009JC005512, 2010.
Vilibić, I.: An analysis of dense water production on the North Adriatic shelf, Estuar. Coast. Shelf S., 56, 697–707, 2003.
Vilibić, I. and Orlić, M.: Least-squares tracer analysis of water masses in the South Adriatic (1967–1990), Deep-Sea Res. Pt. I, 48, 2297–2330, 2001.
Vilibić, I., Mihanović, H., Šepić, J., and Matijević, S.: Using self-organising maps to investigate long-term changes in deep Adriatic water patterns, Cont. Shelf Res., 31, 695–711, 2011.

OSD
11, 331–390, 2014

Qualified climatologies in a changing Adriatic Sea

M. Lipizer et al.

Vilibić, I., Matijević, S., Šepić, J., and Kušpilić, G.: Changes in the Adriatic oceanographic properties induced by the Eastern Mediterranean Transient, Biogeosciences, 9, 2085–2097, doi:10.5194/bg-9-2085-2012, 2012.
Vilibić, I., Šepić, J., and Proust, N.: Weakening thermohaline circulation in the Adriatic Sea, Clim. Res., 55, 217–225, doi:10.3354/cr01128, 2013.
Wolf, J. and Luksch, J.: Physicalische Untersuchungen in adriatischen und sicilisch jonischen Meere wärend des Sommers 1880 an Bord des Dampfers "Hertha". Beillage zu Mitteailungen aus dem Gebiete des Seeswesens, 8, 1–79, 1881.
Zavatarelli, M., Raicich, F., Bregant, D., Russo, A., and Artegiani, A.: Climatological biogeochimical characteristics of the Adriatic Sea, J. Marine Syst., 18, 227–263, 1998.

Table 1. Uncertainty *u* associated with climatological maps of temperature, salinity and dissolved oxygen, expressed as percentage misfit (%), represented as the median and 95th percentile misfit of the seasonal maps. Bold indicates the highest median and 95th percentile for each variable.

	Level	Winter		Spring		Summer		Autumn	
		Median	95 %	Median	95 %	Median	95 %	Median	95 %
Temperature	0 m	4.6	18.9	**14.9**	**27.9**	5.6	12.5	11.7	27.6
	50 m	2.8	9.5	3.8	9.2	3.8	9.3	4.8	12.2
	100 m	2.5	7.8	3.1	7.3	3.3	4.2	3.3	8.3
	200 m	1.4	4.9	1.8	4.9	2.0	5.6	2.2	5.3
Salinity	0 m	0.9	8.4	1.3	8.1	**2.1**	8.8	1.2	**10.2**
	50 m	0.3	0.8	0.3	0.9	0.4	0.9	0.3	0.8
	100 m	0.2	0.6	0.2	0.6	0.2	0.8	0.2	0.5
	200 m	0.1	0.4	0.1	0.4	0.1	0.4	0.1	0.4
Dissolved oxygen	0 m	6.1	**51.6**	6.4	26.3	6.0	34.3	7.0	32.9
	50 m	5.9	34.8	4.3	50.8	7.7	39.2	9.0	51.1
	100 m	11.4	44.0	3.9	50.7	5.0	50.7	6.1	51.2
	200 m	14.2	35.7	4.7	50.6	5.6	46.8	**18.5**	50.9

OSD
11, 331–390, 2014

Table A1. List of the projects and the institutes which have provided the data used in this study.

Project	Period	Institute
AAS	1990–1994	CNR, Istituto di Biologia del Mare, Venezia
ADRIA	1971–1973	OGS, Dipartimento di Oceanografia, Trieste
ADRICOSM/ADRICOSM-EXT	2001–2006	ARPA Emilia Romagna, Struttura Oceanografica Daphne, Cesenatico
		CNR, Istituto di Ricerche sulla Pesca Marittima, Ancona
		Center for Marine Research, Rovinj
		ENEA,Centro Ricerche Ambiente Marino, La Spezia
		Institute of Oceanography and Fisheries, Split
		Laboratorio di Biologia Marina, Trieste
		National Institute of Biology, Piran
		OGS, Dipartimento di Oceanografia, Trieste
ASCOP	1979–1991	CNR, Istituto Sperimentale Talassografico, Trieste
		CNR, Istituto di Biologia del Mare, Venezia
		CNR, Istituto di Ricerche sulla Pesca Marittima, Ancona
		OGS, Dipartimento di Oceanografia, Trieste
DINAS/DIGOT	1977–1985	CNR, Istituto Sperimentale Talassografico, Trieste
		OGS, Dipartimento di Oceanografia, Trieste
EGE-MED XBT DATA	1992–1999	Dept. of Navigation, Hydrography and Oceanography, Istanbul
EGITTO-1	2005	OGS, Dipartimento di Oceanografia, Trieste
EUROMARGE-AS	1993–1996	CNR, Istituto per la Geologia Marina, Bologna
International Biological Project	1965–1965	CNR, Istituto di Biologia del Mare, Venezia
MAST III/MTP II/MATER	1997–1999	CNR, Istituto Sperimentale Talassografico, Trieste
		CNR, Istituto di Ricerche sulla Pesca Marittima, Ancona
		OGS, Dipartimento di Oceanografia, Trieste
MAT	1999–2003	CNR, Istituto di Ricerche sulla Pesca Marittima, Ancona
MFSPP/MFSTEP	1998–2006	ENEA,Centro Ricerche Ambiente Marino, La Spezia
		OGS, Dipartimento di Oceanografia, Trieste
National oceanographic program	2000	Institute of Oceanography and Fisheries, Split
OSO (OPEN SEA OCEANOGRAPHY)	1989	National Centre for Marine Research, Athens
OSO, MEDPOL	1988–1989	National Centre for Marine Research, Athens
OTRANTO	1993–1996	CNR, Istituto Sperimentale Talassografico, Trieste
		National Centre for Marine Research, Athens
		OGS, Dipartimento di Oceanografia, Trieste
PAA	1995–1998	CNR, Istituto di Biologia del Mare, Venezia
PCO	1986–1989	CNR, Istituto di Biologia del Mare, Venezia
PFP	1978–1979	CNR, Istituto di Biologia del Mare, Venezia

OSD
11, 331–390, 2014

Table A1. Continued.

Project	Period	Institute
POEM/POEM-BC	1984–1998	CNR, Istituto Sperimentale Talassografico, Trieste
		CNR, Istituto di Biologia del Mare, Venezia
		CNR, Istituto di Ricerche sulla Pesca Marittima, Ancona
		Division of Applied Sciences, Harvard University, Cambridge
		Institut fur Umwelt Physik, Bremen
		Institute of Oceanography and Fisheries, Split
		National Centre for Marine Research, Athens
		OGS, Dipartimento di Oceanografia, Trieste
PRISMA-1/PRISMA-2	1994–1998	CNR, Istituto Sperimentale Talassografico, Trieste
		CNR, Istituto di Ricerche sulla Pesca Marittima, Ancona
		OGS, Dipartimento di Oceanografia, Trieste
		CNR, Istituto Studio Dinamica Grandi Masse, Venezia
		CNR, Istituto di Biologia del Mare, Venezia
PRV	1986–1990	CNR, Istituto di Biologia del Mare, Venezia
SARI	1994–1995	Stazione Zoologica, Napoli
SESAME	2006–2008	OGS, Dipartimento di Oceanografia, Trieste
Southern Adriatic	1990–1991	CNR, Istituto Sperimentale Talassografico, Trieste
UNKNOWN	1964	Akademia e Shkencave, Tirane
	1972	CNR, Istituto Studio Dinamica Grandi Masse, Venezia
	1966–1972	CNR, Istituto di Biologia del Mare, Venezia
	1977–1981	CNR, Istituto di Ricerche sulla Pesca Marittima, Ancona
	1983–1984	CNR, Istituto Oceanografia Fisica, La Spezia
	1911–1914	Commissione Permanente per lo Studio dell'Adriatico, Venezia
	1974–1997	Croatian Hydrographic Institute, Split
	1979	IO RAS, Institute of Oceanology of the Russian Academy of Sciences
	1913–1999	Institute of Oceanography and Fisheries, Split
	1972	Israel Oceanographic and Limnological Research, Haifa
	1975–1985	Istituto Idrografico della Marina, Genova
	1977	MSU, Moscow State University
	1991	OB-SOI, Odessa Brunch of State Oceanography Institute, Ukraine
	1969	OGS, Dipartimento di Oceanografia, Trieste
	1958–1978	Observatoire Oceanologique de Villefranche-Sur-Mer
	1977	POI, Pacific Oceanological Institute, Vladivostok
	1911–1914	Permanente Internationale Kommission fuer die Erforschung der Adria, Wien
	1966	SHOM, Musee Oceanographique de Monaco
	1958	Southern Scientific Research Institute of Marine Fisheries and Oceanography
	1990	UKRNCES, UKRainian National Center of Ecology of Seas, Ukraine
	1908–1993	UNKNOWN
	1962	Woods Hole Oceanographic Institution, MA
VECTOR	2006–2009	OGS, Dipartimento di Oceanografia, Trieste

Table A2. List of acronyms.

AdDW	Adriatic Deep Water
AOU	Apparent Oxygen Utilisation
BiOS	Bimodal Oscillating System
COM	Climatology-Observations Misfit
DIVA	Data-Interpolating Variational analysis
DO	dissolved oxygen
EAC	Eastern Adriatic Current
EMDW	Eastern Mediterranean Deep Water
EMT	Eastern Mediterranean Transient
FEM	Finite Element Method
IQR	interquartile range
ISW	Ionian Surface Water
MAdG	Mid-Adriatic Gyre
MAdP	Mid Adriatic Pits
MAW	Modified Atlantic Water
MK	Mann-Kendall
MLIW	Modified Levantine Intermediate Water
MSFD	Marine Strategy Framework Directive
NAdDW	North Adriatic Dense Water
NAdG	North Adriatic Gyre
NODC	National Oceanographic Data Centre
OCV	Ordinary Cross Validation
OI	Optimal Interpolation
QC	Quality Control
ROFI	Region of Freshwater Influence
S	Salinity
SAdG	South Adriatic Gyre
SAdP	South Adriatic Pit
SNR	Signal to Noise ratio
SST	Sea Surface Temperature
T	Temperature
VIM	Variational Inverse Method
WAC	Western Adriatic Current
WFD	Water Framework Directive

OSD
11, 331–390, 2014

Qualified climatologies in a changing Adriatic Sea

M. Lipizer et al.

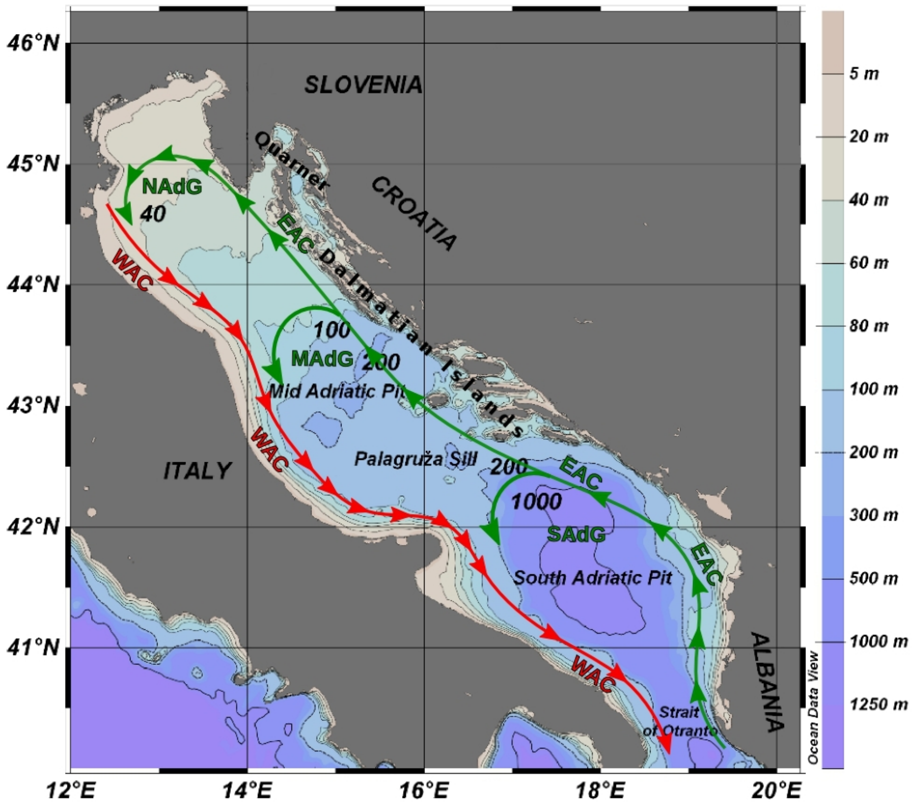

Fig. 1. Adriatic Sea: bathymetry, morphology and main surface circulation (redrawn with modifications from Poulain and Cushman-Roisin, 2001). Acronyms as defined in the List of acronyms.

OSD
11, 331–390, 2014

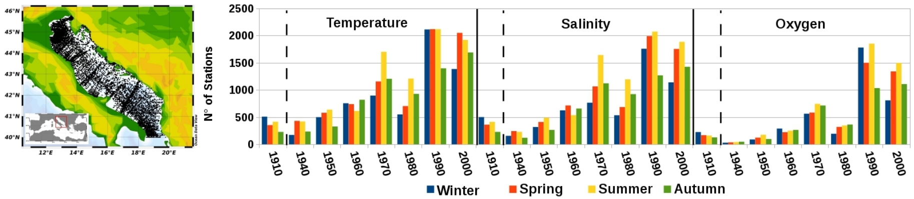

Fig. 2. Geographical distribution of stations (left) and number of stations per decade, season and variable (right).

OSD
11, 331–390, 2014

Qualified climatologies in a changing Adriatic Sea

M. Lipizer et al.

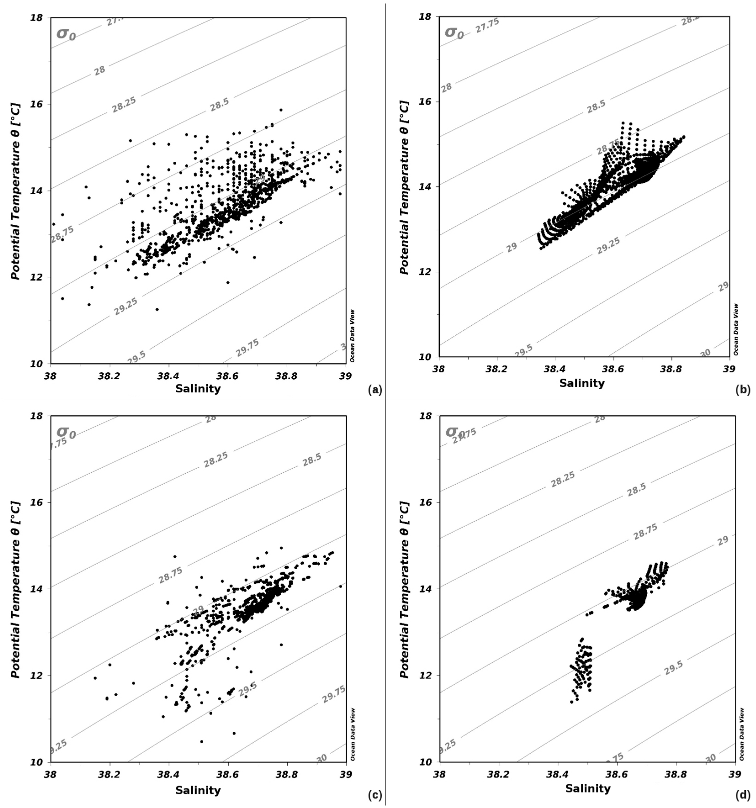

Fig. 3. Comparison of *TS* diagrams based on in situ **(a)** and reconstructed data **(b)** in summer (100 m) and in winter (200 m) (**c**, in situ) and (**d**, reconstructed).

OSD
11, 331–390, 2014

Qualified climatologies in a changing Adriatic Sea

M. Lipizer et al.

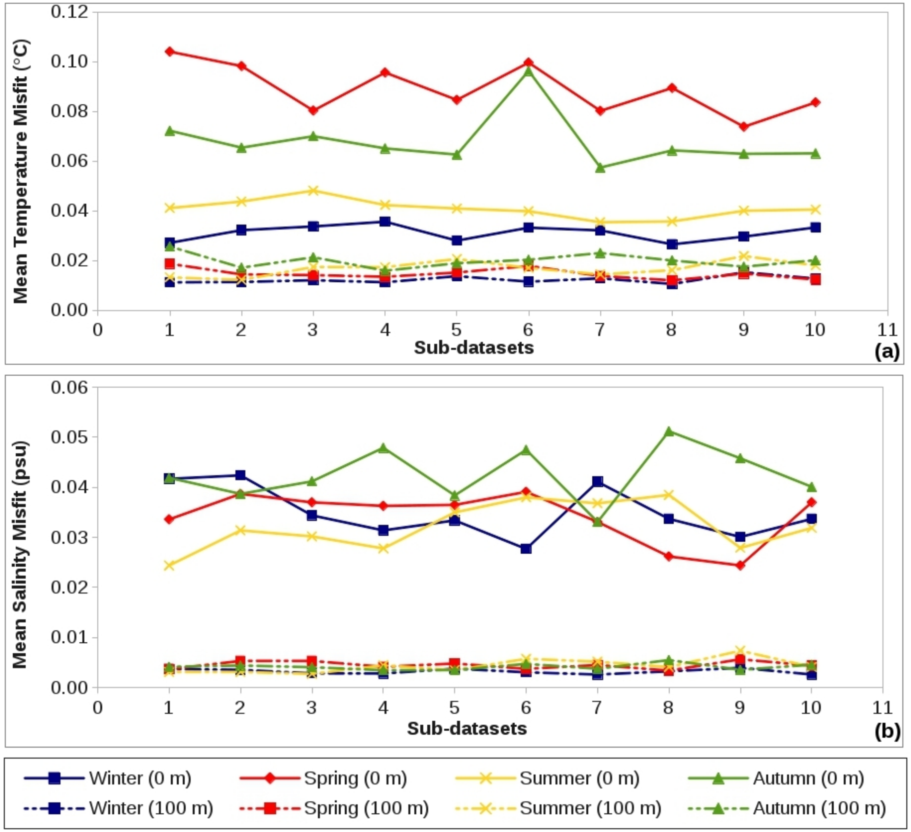

Fig. 4. Mean misfit in temperature **(a)** and in salinity **(b)** in the surface layer (solid lines) and at 100 m depth (dashed lines) derived from Ordinary Cross Validation.

OSD
11, 331–390, 2014

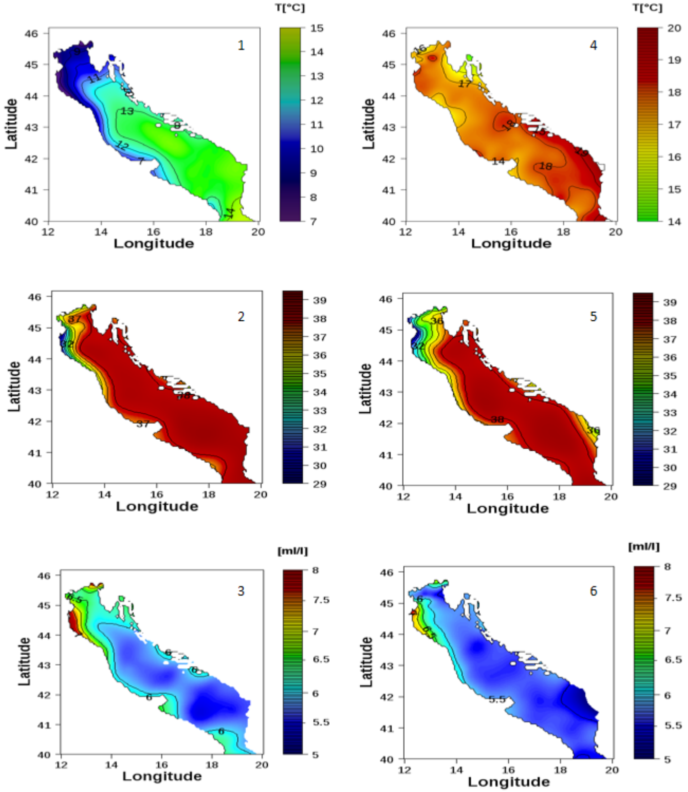

Fig. 5. Climatological maps of surface of temperature (1, 4), salinity (2, 5) and dissolved oxygen (3, 6) in winter (left) and spring (right).

OSD
11, 331–390, 2014

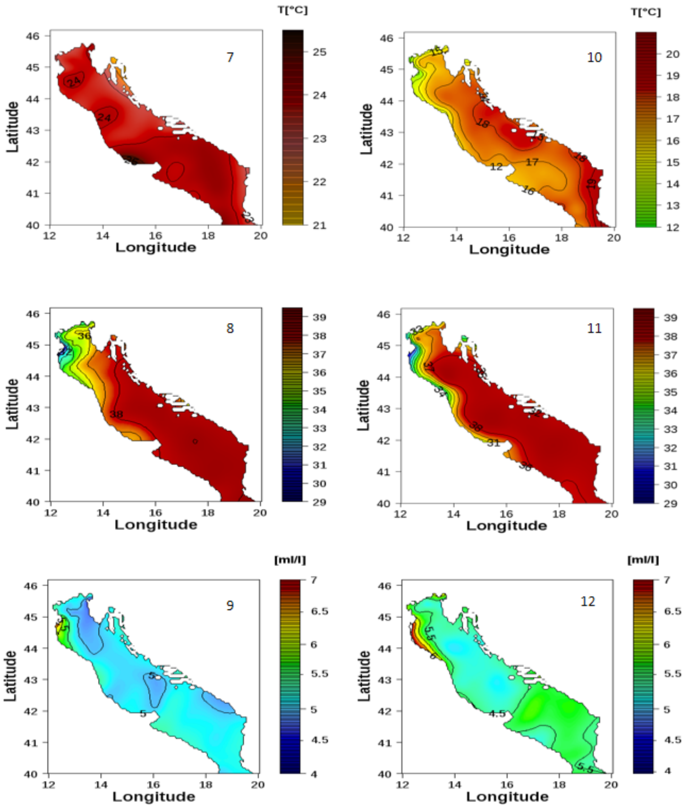

Fig. 5. Climatological maps of surface of temperature (7, 10), salinity (8, 11) and dissolved oxygen (9, 12) in summer (left) and autumn (right).

OSD
11, 331–390, 2014

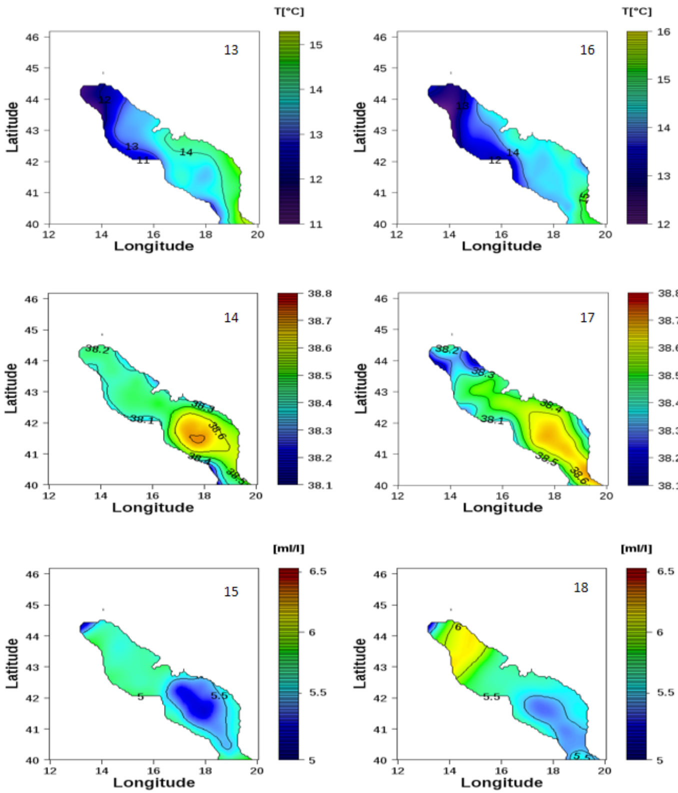

Fig. 5. Climatological maps at 50 m of temperature (13, 16), salinity (14, 17) and dissolved oxygen (15, 18) in winter (left) and spring (right).

OSD
11, 331–390, 2014

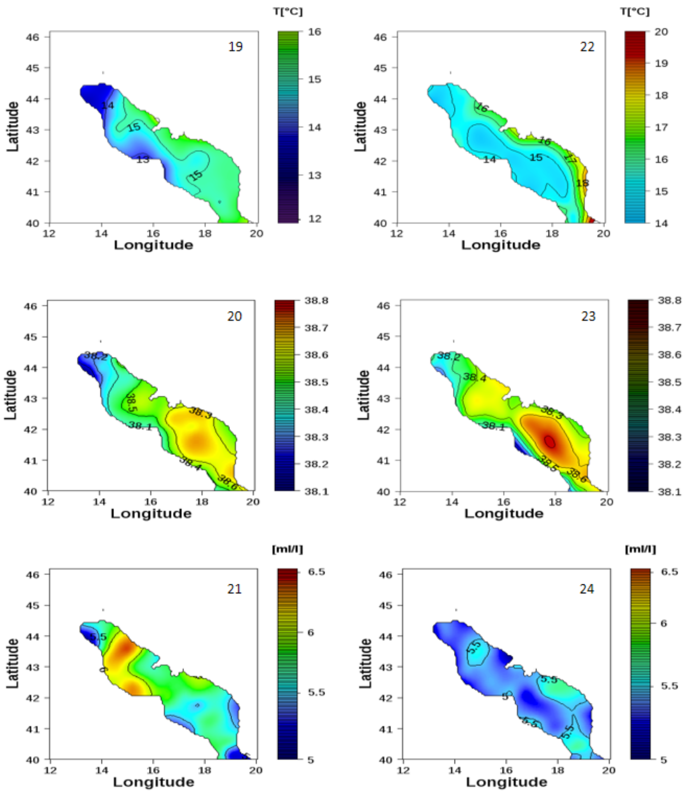

Fig. 5. Climatological maps at 50 m of temperature (19, 22), salinity (20, 23) and dissolved oxygen (21, 24) in summer (left) and autumn (right).

OSD
11, 331–390, 2014

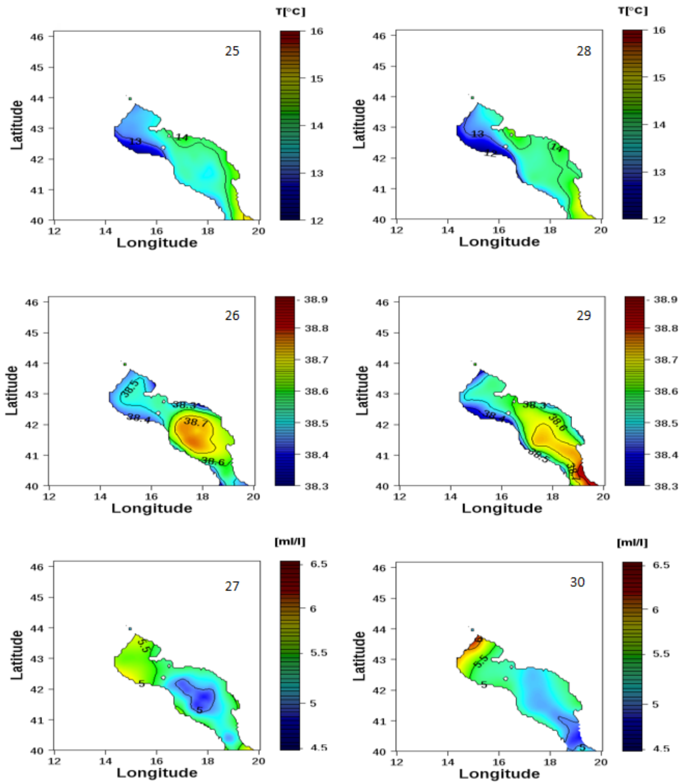

Fig. 5. Climatological maps at 100 m of temperature (25, 28), salinity (26, 29) and dissolved oxygen (27, 30) in winter (left) and spring (right).

OSD
11, 331–390, 2014

Qualified climatologies in a changing Adriatic Sea

M. Lipizer et al.

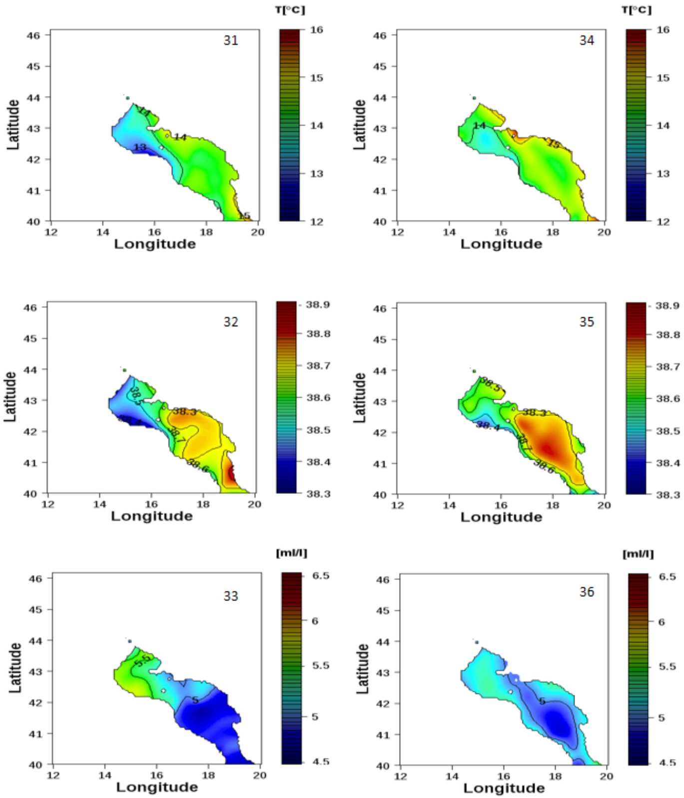

Fig. 5. Climatological maps at 100 m of temperature (31, 34), salinity (32, 35) and dissolved oxygen (33, 36) in summer (left) and autumn (right).

OSD
11, 331–390, 2014

Qualified climatologies in a changing Adriatic Sea

M. Lipizer et al.

Title Page
Abstract | Introduction
Conclusions | References
Tables | Figures
◀| |▶
◀ ▶
Back | Close
Full Screen / Esc
Printer-friendly Version
Interactive Discussion

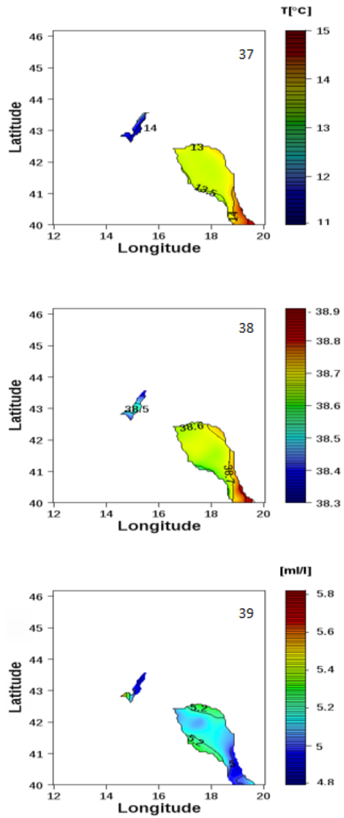

Fig. 5. Climatological maps of the 200 m layer of temperature (37), salinity (38) and dissolved oxygen (39) in spring.

OSD
11, 331–390, 2014

Qualified climatologies in a changing Adriatic Sea

M. Lipizer et al.

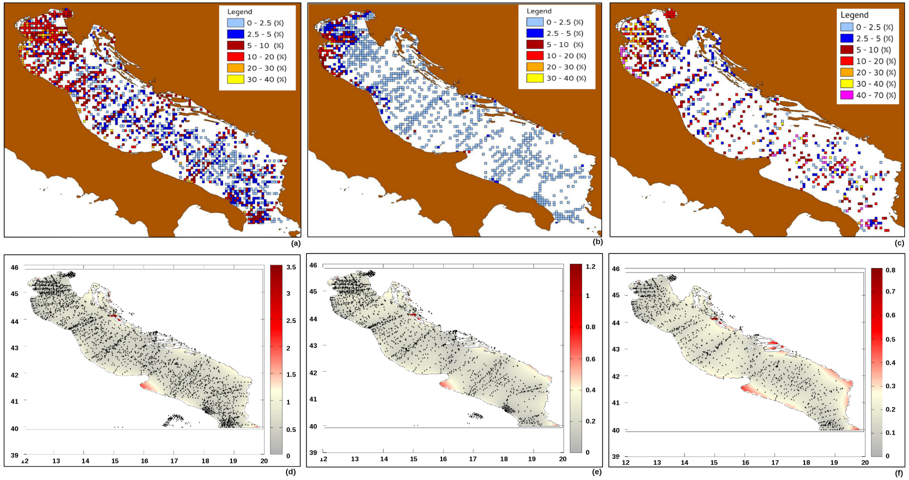

Fig. 6. Uncertainty u maps in winter of surface temperature **(a)**, salinity **(b)** and oxygen **(c)** climatology (expressed as percentage deviation from the approximation). Measurement locations are displayed on the error field e maps of temperature **(d)**, salinity **(e)** and oxygen **(f)**, expressed as °C, salinity unit and $\mathrm{mL\,L^{-1}}$, respectively. Colour scales are indicated in each map.

OSD
11, 331–390, 2014

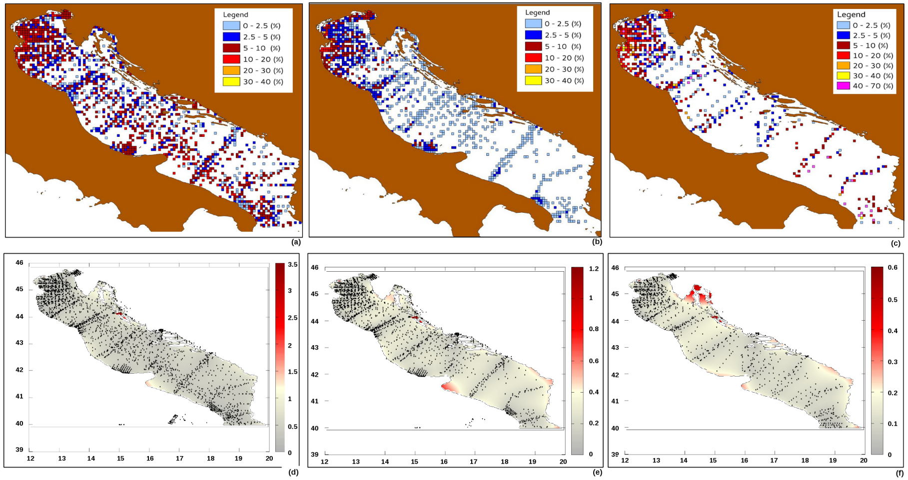

Fig. 7. As in Fig. 6 for summer.

OSD
11, 331–390, 2014

Qualified climatologies in a changing Adriatic Sea

M. Lipizer et al.

Title Page
Abstract | Introduction
Conclusions | References
Tables | Figures
◂◂ | ▸▸
◂ | ▸
Back | Close
Full Screen / Esc
Printer-friendly Version
Interactive Discussion

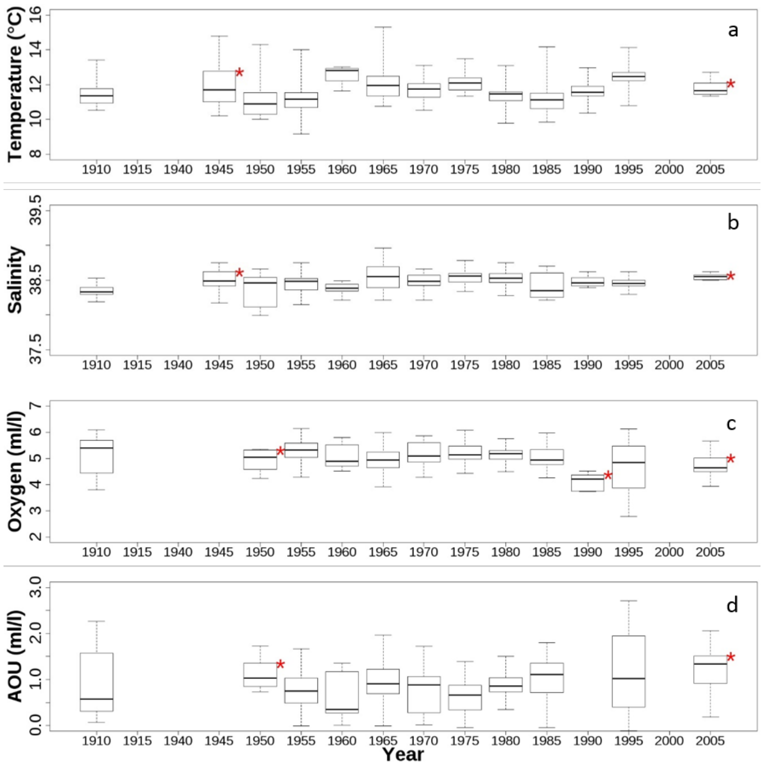

Fig. 8. Box plots show the five-year median (line), interquartile range (IQR, box) and extremes (whiskers) of temperature **(a)**, salinity **(b)**, dissolved oxygen **(c)** and AOU **(d)** in the deep waters of the Middle Adriatic. Asterisks (*) indicate when statistics are based on less than 3 yr of data. The year on the x-axis indicates the beginning of the 5 yr period.

OSD
11, 331–390, 2014

Qualified climatologies in a changing Adriatic Sea

M. Lipizer et al.

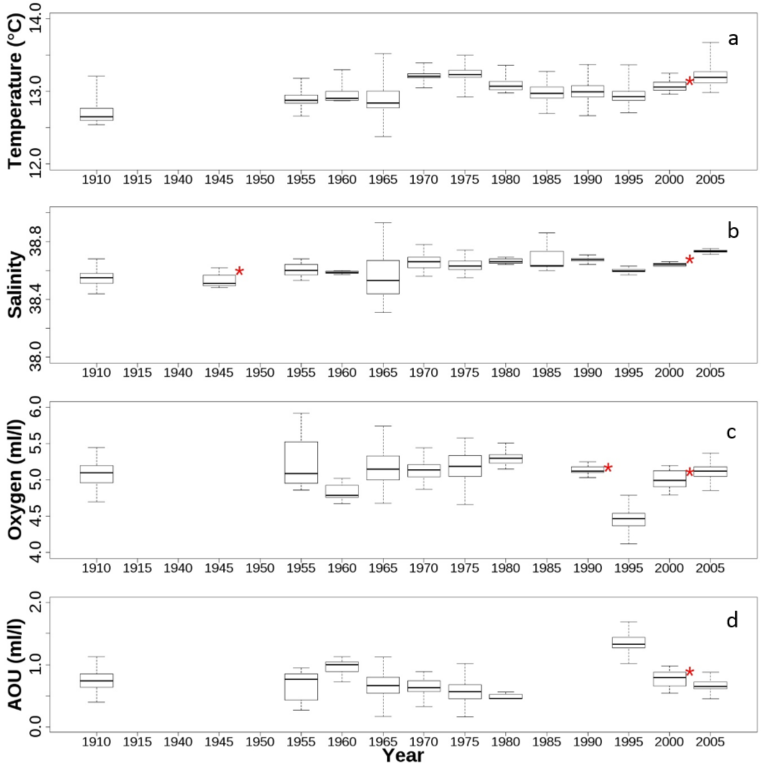

Fig. 9. As in Fig. 8, for the South Adriatic.

OSD
11, 331–390, 2014